

Czech Technical University in Prague
Faculty of Mechanical Engineering

Department of Automotive, Combustion Engine and Railway Engineering
Study program: Master of Automotive Engineering
Field of study: Advanced Powertrains



Scavenged Pre-chamber for a
Light-Duty Truck Gas Engine

DIPLOMA THESIS

Author: Bc. Jan Andres
Supervisor: Ing. Jiří Vávra, Ph.D
Specialist: Ing. Zbyněk Syrovátka
Year: 2016

Disclaimer

I hereby declare that this thesis is my own work and that to the best of my knowledge and the bibliography contains all the literature I have used. It contains no materials previously published or written by another person, or substantial proportions of material which have been accepted for the award of any other degree or diploma at CTU or any other educational institution, except where due acknowledgement is made in the thesis.

.....
Date

.....
Bc. Jan Andres

Acknowledgment

Foremost, I would like to express my sincere gratitude to my supervisor Ing. Jiří Vávra, PhD. for continuous support of my Master thesis, for his patience, motivation and knowledge. His guidance helped me in all the time of writing the thesis. Beside my supervisor, I would like to thank to my specialist Ing. Zbyněk Syrovátka for his patience and priceless advices during writing the thesis. My sincere thanks also goes to prof. Ing. Michal Takáts, CSc, doc. Oldřich Vítek, Ph.D, Ing. Radek Tichánek, Ph.D and my colleagues at the Research and Scientific Park. Last but not the least, I would like to thank my family for supporting throughout studies.

Bc. Jan Andres

Author: Bc. Jan Andres

Title: **Scavenged Pre-chamber for a Light-Duty Truck Gas Engine**

Study program: Master of Automotive Engineering

Field of study: Advanced Powertrains

Assignment: Diploma Thesis

Scope of the Thesis: 83 pages, 50 figures, 2 tables, 42 attachments

Academic Year: 2015/2016

Department: U 12120

Supervisor: Ing. Jiří Vávra, Ph.D
Czech Technical University in Prague
Faculty of Mechanical Engineering
Technická 4, 166 07 Praha 6 - Dejvice, Czech Republic

Josef Bozek Research Centre for Vehicles of Sustainable Mobility
Scientific and Technical Park
Přílepská 1920, 252 63 Roztoky u Prahy

Specialist: Ing. Zbyněk Syrovátka
Czech Technical University in Prague
Faculty of Mechanical Engineering
Technická 4, 166 07 Praha 6 - Dejvice, Czech Republic

Josef Bozek Research Centre for Vehicles of Sustainable Mobility
Scientific and Technical Park
Přílepská 1920, 252 63 Roztoky u Prahy

Abstract: The thesis deals with the 3-D CAD model of the pre-chamber ignition system as well as drawings created in the software PTC Creo for an engine which is able to burn compressed natural gas. The aim is to create a modular pre-chamber system using mass produced parts. The CAD model is used to create a 3-D CFD model in the software AVL Fire. The parametric design of the model saves a time with creating each iteration. The 3-D CFD model shows what happens inside the chamber during the cycle and where is a space for ongoing improvements of the design to increase the efficiency, decrease the fuel consumption and decrease costs.

Key words: Pre-chamber, CNG, Indirect injection, 3-D CAD, 3-D CFD, Lean mixture

Contents

Nomenclature	8
1 Preface	10
2 Literature Search	13
2.1 Natural Gas	16
2.2 Pre-chamber Ignition System	19
2.2.1 Mahle - Turbulent Jet Ignition	19
2.2.2 MWM GmbH	22
2.2.3 CKD	23
2.2.4 GE Jenbacher GmbH	24
2.3 Daewoo-Avia D432 Engine	25
2.3.1 Engine Modification to SI	27
2.3.2 Original CTU Scavenged Pre-chamber Design	27
3 Design Part	31
3.1 Cylinder Head	31
3.2 Module Housing	33
3.3 Spark Plug Socket	36
3.4 Insertion	38
3.5 Gas Elbow	39
3.6 Upper Housing	40
3.7 Purchased parts	41
3.7.1 Spark Plug	41
3.7.2 Miniature Pressure Transducer	42
3.7.3 Ball Check Valve	43

3.8	Complete Assembly	44
3.9	Version Without the Pressure Transducer	47
4	3-D CFD Part	52
4.1	CFD Model	56
4.2	Results	59
5	Conclusion	63
	References	65
	List of Figures	69
	List of Tables	69
	List of Attachments	70

Nomenclature

ℓ	Turbulent Length Scale
ϵ	Dissipation per Unit Mass
λ	Stoichiometry Ratio
μ	Dynamic Viscosity
μ_T	Eddy Viscosity
ν	Kinematic Viscosity
\bar{A}	Time Averaged Turbulent Quantity
ρ	Density
τ_{ij}	Reynolds Stress Tensor
A'	Turbulent Fluctuating Part
$D \cdot n$	Normal Component of Deformation Tensor
S_{ij}	Mean Strain Tensor
$T \cdot n$	Normal Component of the Stress Tensor
$u \cdot n$	Normal Component of Velocity
3-D	Three Dimensional
BDC	Bottom Dead Center
BMEP	Break Mean Effective Pressure
CAD	Computational Aided Design
CFD	Computational Fluid Dynamics
CHP	Combined Heat and Power
CNG	Compressed Natural gas
CO	Carbon Monoxide

CO ₂	Carbon Dioxide
DNS	Direct Numerical Solution
e	Kinetic Energy
EGR	Exhaust Gas Recirculation
f	Force Acting on the Control Volume
HC	Hydrocarbon
k	Specific Kinetic Energy
L	Characteristic Length
LES	Large Eddy Simulation
LNG	Liquefied Natural Gas
m	Mass
N	Nitrogen
NGL	Natural Gas Liquid
NO	Nitric Monoxide
NO ₂	Nitrogen Dioxide
NO _x	Nitric Oxide
p	Static Pressure
PFI	Port Fuel Injection
PPM	Parts Per Million
PTFE	Poly Tetra Fluor Ethylene
RANS	Reynolds Averaged Navier-Stokes
Re	Reynolds Number
RPM	Revolutions per Minute
t	Time
TDC	Top Dead Center
TJI	Turbulent Jet Ignition
U	Internal Energy
V	Volume

Chapter 1

Preface

One of the most challenging nowadays task for automotive manufacturers all around the world is to decrease emissions of their cars. There are actually two main reasons why they have to deal with it. First is a legislative and high fines in case of not meeting the target and second one is to bring something special to the high competitive market and gain an advantage over the competitors. It is already visible that the main manufacturers try to include alternative fuels or electric cars to their portfolio because the development of current engines is expensive and the improvement is not that high, especially at diesel engines. Natural gas as an alternative fuel would be one of the opportunities how to satisfy legislative norms as well as offer a deal for costumers by lower costs per kilometre. The support of natural gas in the future can be caused by theoretical higher supply than crude oil all around the world. Moreover, natural gas is supported by governments as a cleaner fuel for mobility. Natural gas in its pure form is colorless, odourless and mainly combustible. It consists primarily of methane. It also contains higher hydrocarbons. The composition of the natural gas is little bit different at each deposit [18]. Natural gas in the automotive industry is used in a form of CNG (Compressed Natural Gas) or LNG (Liquefied Natural Gas). The technical advantage of the natural gas is that it is burnt at a very lean mixture which decrease the amount of CO₂ due to higher amount of air and decrease NO_x due to lower temperature of the flame. It has high octane number around 130, which decreases the possibility of knocking and increase the power of the engine. No soot is created during combustion [18].

The literature search part of the thesis focuses on principles of an indirect injection, advantages of a lean mixture combustion, chemical elements created during combustion and how they affect the environment and the human health [6]. In general, it shows the CNG fuel, its extraction, a chemical composition and reasons why CNG is suitable as a fuel for the automotive industry [14]. The composition of the gas also influences the performance of the vehicle [23]. Last but not least is an overview of already existing variants of an indirect pre-chamber ignition systems like CKD [19], MWM [12], Mahle [2] and GE [5]. Then a basic overview of an engine D432 which is used for the experiment and which was originally mounted in the light-duty truck Daewoo Avia [3]. The same series of an engine was used by the company Tedom a.s. The idea was to use the engine as the Combined Heat and Power plant (CHP). The thesis also describes the last designed by my predecessor [21].

The first aim of the thesis is to create a brand new CAD model of the pre-chamber module which will be installed in the experimental gas engine. The thesis connects on the thesis of my predecessors [8], [19]. Nowadays, there is already a functional solution designed by my predecessor [21]. It means that experimental data are available and it gave a baseline for requirements for a new design. The design part deals with a simplification and the modularity of the product by using mass produced parts and optimization of the space. The thesis describes an engine, each part of a module in detail, a gas supply, a pressure measurement and a sealing. It is required to use a mass produced cylinder head and do only minimum changes in its design. The spark plug is also mass produced. There are two main problems with the original design and both are due to limited space around the spark plug. One of them is that the spark plug is eccentrically mounted and another one is that the original spark plug is modified. Only a ceramic insulator with a central electrode is used thus both the ground electrode and the center electrode are not in the ideal position to each other. Usually the ground electrode is approximately 1 mm under the center electrode but here the ground electrode is mounted next to the center electrode. The detail of the original design is shown in the figure 1.1. The detailed description is in the chapter "Original CTU Scavenged Pre-chamber Design" where is also shown the ceramic insulator and the center electrode 2.17. The ideal spark in not achieved in this case and that is why a mass produced centrally mounted spark plug without any adjustment is required.

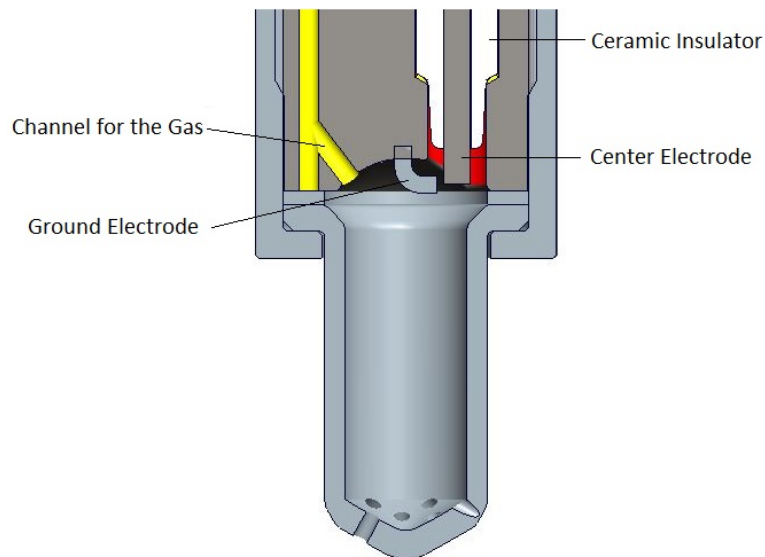


Figure 1.1: Position of the spark plug [21]

The new design should include a symmetrical distribution of a gas to achieve better scavenging of residual gases after combustion. The channel for a symmetric distribution of the fuel should be created as close as possible to the combustion chamber to avoid useless negative volume. Gas has to be supplied through a side channel in the cylinder head which was originally used for fuel supply. The ball check valve is used to control the gas flow and it should be positioned near to the combustion chamber.

The second aim is to create and test a 3-D CFD model of a pre-chamber which gives a deeper understanding of processes inside the chamber. The model focuses on a scavenging and leakages of methane during an expansion stroke. The data are based on an experiment for validating the 1-D model created in a software GT-Power. The CFD model is configured based on these data. Unfortunately, the data are valid for the original design, hence the 3-D CFD model is based on the original design too. The same data are in parallel used for creating similar model using the software Ansys Fluent [20]. The data should be analyzed and compared but it is not a scope of the thesis. The theoretical part of CFD is based on the literature [22], [4], [7] and [24]. In this stage the 3-D CFD model does not include the combustion. If the model works correctly based on the GT-Power model, it will be used for further improvements of the combustion chamber design. Thus, it will be possible to modify the design and compare many variants to increase efficiency and decrease fuel consumption. The simulations also brings lower costs because it is not necessary to produce expensive prototypes.

Chapter 2

Literature Search

The indirect injection system is a fuel injection system where the fuel is not injected directly to the combustion chamber. There are several possibilities how to transport the fuel to the combustion chamber. The typical arrangement of gas engines is that the fuel is injected to the intake manifold where it is mixed with air and then the mixture enters the combustion chamber. The second possibility is to use the pre-chamber system or the swirl chamber system where the combustion begins. Then, the lean mixture is injected to the main combustion chamber. The literature search focuses on a design of different pre-chamber systems. The literature research also focuses on the natural gas and its composition and the impact on the combustion and emissions. The main aim of the lean combustion is a low temperature combustion to achieve low emission of NOx ideally without following after treatment in the catalytic converter. The principle is to provide a rapid burn of the lean mixture inside the combustion chamber which requires a high energy for the ignition. The ignition energy of the pre-chamber ignition system is several times higher than the ignition energy of a typical spark plug. Moreover, the combustion starts at multiple locations simultaneously. The concept of the lean combustion increases efficiency due to the Poisson ratio [6].

$$\eta = \frac{W}{Q_P} = 1 - \frac{1}{CR^{\kappa-1}} \quad (2.1)$$

η ...Thermal efficiency [-]

W ...Work [J]

Q_P ...Supplied heat [J]

CR ...Compression Ration [-]

κ ...Poisson ratio [-]

The equation says that the difference between two similar engines is given by Poisson ratio. The higher Poisson ration the higher efficiency. The heat capacity at constant pressure has to be higher than the heat capacity at constant volume thus the Poisson ratio is higher than 1 [6].

$$\kappa = \frac{c_P}{c_V} \quad (2.2)$$

c_P ...Specific heat capacity at constant pressure $\left[\frac{J}{K} \right]$

c_V ...Specific heat capacity at constant volume $\left[\frac{J}{K} \right]$

The Maier relation for the heat capacity at constant pressure.

$$c_P = c_V + r \quad (2.3)$$

r ...Specific gas constant $\left[\frac{J}{Kg \cdot K} \right]$

The relation for the Poisson ratio is in the following equation.

$$\kappa = \frac{c_V + r}{c_V} \quad (2.4)$$

The specific heat capacity at constant volume c_V increases with the temperature thus the Poisson ratio κ decreases with the temperature. The Poisson ratio depends on the type of the gas. The more atoms in the gas the lower Poisson ratio. It shows that the lean mixture is convenient because air consist primarily of N_2 and O_2 . The Poisson ratio for air is 1,4. In a low load regime is not necessary to restrict the intake of air It decreases pumping losses. The mixture is possibly diluted by EGR gases, which decrease the temperature of the mixture, hence decrease the amount of nitrogen oxides NO_x . In the figure 2.1 is a scheme of the pre-chamber [6].

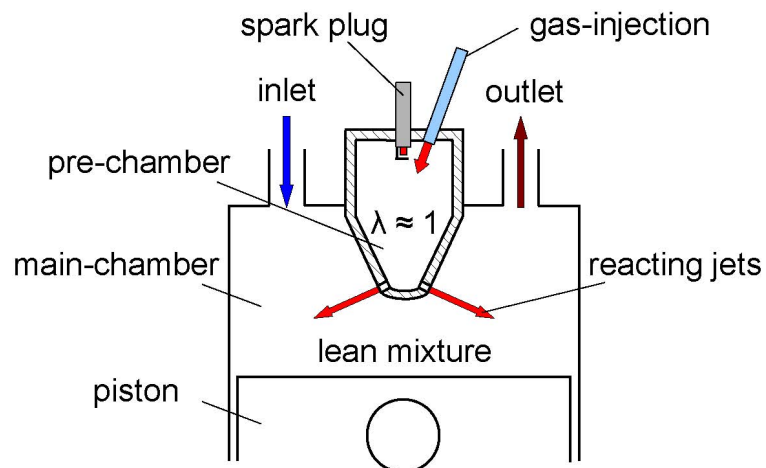


Figure 2.1: Pre-chamber scheme

The pre-chamber has usually a volume up to several % of the main combustion chamber volume. The experimental engine is the four stroke engine. In general, during the intake stroke inlet valve opens and the fresh mixture enters the cylinder while piston moves downward. The fresh gas is also injected into the pre-chamber. During the compression stroke piston goes up, both valves are closed and the mixture from the cylinder is pushed into the pre-chamber and dilutes the gas. Few degrees of the crank shaft before the TDC, a spark is generated and the combustion begins. The pressure is increasing rapidly. During an expansion stroke the pressure is rising up for a few degrees of the crankshaft but while the piston goes down, pressure decreases and burning mixture is forced out of the pre-chamber. The connection between the pre-chamber and the combustion chamber is given by small orifices. The function of these orifices is to enable the burning fuel enter the main combustion chamber and spread the flame throughout the main combustion chamber. Another very important feature of these small orifices is to create turbulent flow which penetrate deeper into main charge. The turbulent flow causes faster chemical reactions. The burning mixture ignites a very lean mixture in the combustion chamber. Right before the BDC an exhaust valve opens and during an exhaust stroke burned gas is pushed away from the cylinder by an exhaust valve to an exhaust system. The inlet valve opens a few degrees of the cranskshaft before the TDC and the whole cycle goes again [6].

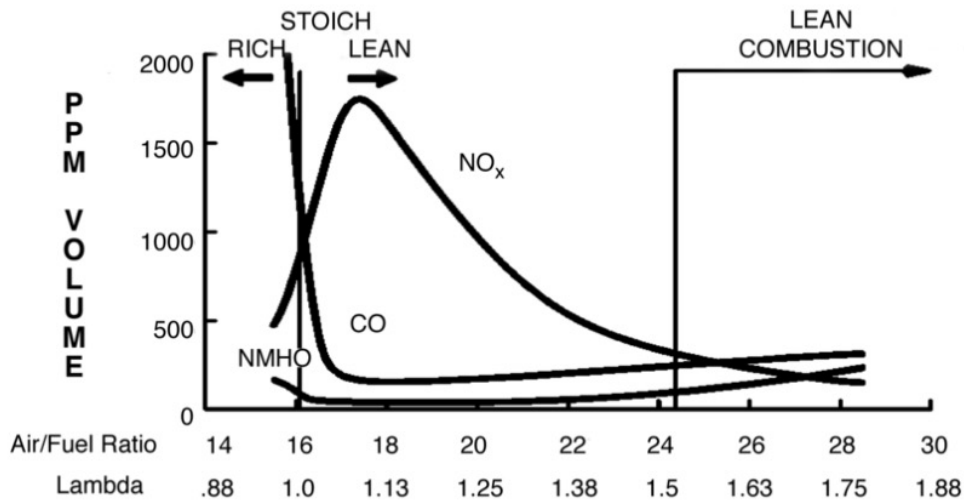


Figure 2.2: Amount of emission versus air/fuel ratio [17]

The main products of the combustion of natural gas are carbon dioxide and water vapour. During combustion is created a very small amount of nitrogen oxides, carbon oxide and almost no ashes or particulate matter. The carbon monoxide CO is controlled primarily by the fuel/air equivalence ratio. Natural gas engines, however, always operate well on the lean side of stoichiometric thus, carbon monoxide emissions are low enough to be unimportant. The carbon dioxide CO_2 is a product of a complete combustion. Nevertheless, it is one of gasses contributing the greenhouse effect. Unburned hydrocarbons HC or more appropriately organic emissions are the consequence of incomplete combustion of the hydrocarbon fuel. Some hydrocarbons

are known as carcinogens [15].

Based on their potential for an oxidant formation in the photochemical smog chemistry, hydrocarbon compounds are divided into non-reactive and reactive categories. In fact, it depends mainly if there is a presence of methane or not. All the hydrocarbons except methane react, given enough time. Crevices are a major source of unburned hydrocarbons. Between a piston and a piston ring, around a spark plug, around an intake and an exhaust valve. The total crevice volume is a few % of the swept volume. If the flame enters the crevice, unburned hydrocarbon will not be created. Another source of unburned hydrocarbon is oil layer deposited on cylinder walls. This layer is scraped off the wall during an exhaust stroke by the piston ring. Some of them is burnt and the rest go on directly to the exhaust manifold. Nitrogen oxides NO_x consist of nitric oxide monoxide NO and nitrogen dioxide NO₂. Nitric oxide is a dominant one and the source is atmospheric nitrogen. Nitric oxide forms in both the flame front and the post-flame gases but dominant formation is in the post-flame. Formation of nitric oxide strongly depends on temperature. Higher temperature and higher oxygen rate are the reason of higher amount of nitric oxide. The peak is at stoichiometry rate. Reaction freezes while the temperature decreases during an expansion stroke. The reaction is usually rapid and quite often nitric oxide is transformed into nitrogen dioxide in an environment with sufficient oxygen and high temperature. The EGR significantly decreases an amount of nitric oxide because these gasses decrease the temperature. The primary effect of the burned gas diluent in the unburned mixture on the nitric oxide formation process is that it reduces flame temperatures by increasing the heat capacity of the cylinder charge, per unit mass of fuel [6].

The figure 2.2 shows NO_x, CO and hydrocarbons emission output versus excess air/fuel ratio and excess air ratio for natural gas engines. Reference oxygen level is 15 %. From this figure it is obvious why is suitable to operate with a very lean mixtures. It is possible to affect the amount of emissions by factors like temperature, dilution of the mixture by fresh air or EGR gases.

2.1 Natural Gas

Extraction of the natural gas can be divided into the onshore and the offshore drilling. The onshore drilling takes place at the earth's surface. There are two main types of onshore drilling. A cable tool drilling and a rotary drilling. The cable tool drilling consists of raising and dropping a heavy metal into the ground which create a hole down through the earth. The cable tool drilling is usually used for shallow, low pressure formations. The rotary drilling consists of a sharp, rotating metal drilling through the Earth's surface. This type of drilling is used primarily for deeper wells, which may be under high pressure. The rotary drilling is modern way how to extract natural gas [14].

The offshore drilling takes place at the sea and it is more challenging because a platform has to be created. The platform can be moveable or permanent. The moveable platform is used at places where the deposit is not too big or just to explore new possible deposits because it is cheaper and this platform can move from

place to place. On the other side, at a place with less depth and with a huge deposit, the permanent platform is used because the extraction is faster. The figure 2.3 shows types of offshore drilling platforms and their depth possibilities [14].

Once a well has been drilled and the presence of commercially viable quantities of a fossil fuel has been verified, the next step is to lift the natural gas out of the ground and processing it for a transportation. The raw natural gas is associated with many other trace gasses, compounds, water and unsuitable oil for a common use. At first, it is necessary to remove these impurities like ethane, propane, butane and pentane. The gases are not waste products, they are used for other purposes. Scrubbers near to the well head are used to remove a sand and other large impurities. Near to the well head are heaters because the temperature should not drop too low. If the temperature drops too much natural gas will hydrate and become a solid. The oil is separated in the separator which is simple closed tank, where the force of the gravity serves to separate the heavier liquids like oil. The removal of the water vapour requires a dehydrating of the natural gas, which usually involves absorption, or adsorption. Absorption occurs when the water vapour is taken out by a dehydrating agent like glycol. Adsorption occurs when the water vapour is

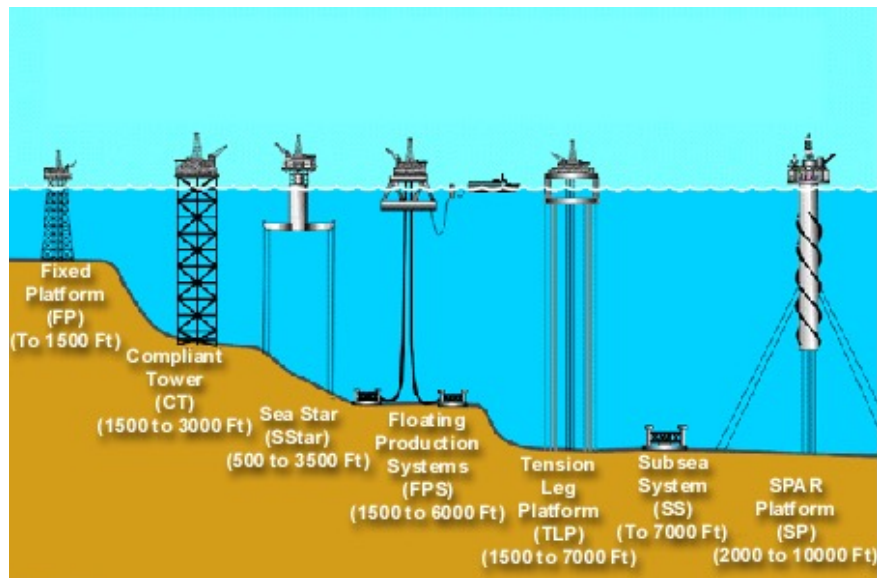


Figure 2.3: Offshore drilling platforms [14]

condensed and collected on the surface. Ethane, propane, butene and pentane, together tagged as NGLs (Natural Gas Liquids) have a higher value as separated products. There are two methods how to separate the NGLs out of the natural gas. The absorption method and the cryogenic expansion process. The absorption method of NGLs extraction is similar to using absorption for dehydration but it uses a agent which has an affinity for NGLs. As the natural gas is passed through an absorption tower, it is brought into contact with the absorption oil which soaks up a high proportion of the NGLs. Now, the oil contains all ethane, propane, butane, pentane and other heavier hydrocarbons. Then the rich oil is heated above the boiling point of the NGLs, but below the boiling point of the oil. However, it can't extract ethane independently. Cryogenic processes can extract the lighter

hydrocarbons, such as ethane. The cryogenic processes consist of dropping the temperature of the gas stream to approximately - 85 °C. This rapid temperature drops condense ethane and other hydrocarbons in the gas stream, while maintaining methane in gaseous form. This process allows for the recovery of about 90 % of the ethane. Last undesirable elements in the natural gas are sulphur and carbon dioxide. Amine solutions are used to remove the hydrogen sulphide. The amine solution has an affinity for sulphur and absorbs it. Now, the pure natural gas continues into pipelines as a dry natural gas to the costumers [14].

Element	Content
CH ₄	98 %
Higher hydrocarbons	1,16 %
CO ₂	0,05 %
N ₂	0,79 %

Table 2.1: Composition of natural gas [18]

Natural gas is one of the cleanest source of energy in nowadays world. Compared to other fossil fuels and emits lower amount of emissions and gives more energy. Natural gas is often associated with oil deposits. In the table 2.1 is a typical composition of natural gas. However, composition of the natural gas slightly varies at each deposit [18].

The team of CTU researchers investigated the influence of natural gas composition on turbocharged stoichiometric SI engine performance under a high load. The engine Avia D432 is modified to be able to burn natural gas and it is described in the following chapter. In this stage the spark ignition engine is a four valve in-line design with a compression ratio 12:1. The fuel mixer is installed in the intake manifold upstream of the compressor. The excess-air ratio is controled to be 1 during the experiments. The power output is 120 kW at 2.000 rpm and the torque output is 600 Nm at 1.600 - 1.800 rpm. Results are as follows. The addition of gaseous higher hydrocarbons increases the power and the efficiency of an engine by an increased mixture volumetric calorific value. On the other side the addition of gaseous higher hydrocarbons worsens the knock resistance and emissions of CO₂ too. The addition of hydrogen decreases emissions of CO₂ but it decreases the engine power and efficiency due to lower calorific value. The hydrogen addition also worsens the knock resistance [23].

To sum up, the advantages far outweigh the disadvantages. Deposits of natural gas are widely diversified all over the World and moreover everyone can build his own filling station at home. This would be a great opportunity for companies with car fleet because they can build a filling station in the area of the company and every day fill all the cars with the best price which is the biggest advantage for a costumers. Natural gas is supported by governments as a clean fuel and costumers pay lower taxes thus the cost for each kilometre is significantly lower. Another important reason for natural gas is the amount in the World which is quite higher than the crude oil. It is possible to use already existing engines and upgrade them to a bi-fuel configuration thus the development is not expensive as well as the development of brand new CNG engine is distinctly cheaper than the development of a hydrogen or an electric car. Natural gas engines offer a possibility to operate with very lean

mixture, hence produce much lower amount of harmful emissions. On the other side, methane is the main element of natural gas and unfortunately, methane is a greenhouse gas. Another disadvantage is that natural gas is a fossil fuel as well as crude oil and that is why we do have only a finite amount but researchers are working on methods how to produce natural gas. So far, there are not sufficient amount of filling stations but the transportation net exists and it is cheaper to build a new CNG filling station than hydrogen or electric stations.

2.2 Pre-chamber Ignition System

The indirect injection is not a new solution and that is why there is an overview of few case studies and the comparison of their advantages and disadvantages. Main differences are seen at design of a pre-chamber and a type of a gas supply. The gas can be injected directly into the pre-chamber or the gas is injected into the combustion chamber and the upward piston movement pushes the gas into the pre-chamber. Some solutions use both injectors in pre-chamber and in the main combustion chamber. Then, it is possible to mix more then one gas like gasoline plus natural gas. Very important parameter is also volume of the pre-chamber.

2.2.1 Mahle - Turbulent Jet Ignition

William Attard and his team made a research in 2010 and as a result they introduced the Turbulent Jet Ignition (TJI) system for an internal combustion engine having at least one combustion chamber with an injector, a spark plug and a pre-chamber where a small amount of charge is ignited and then is used to ignite the main volume of charge in the combustion chamber. Nowadays, this system is pro-

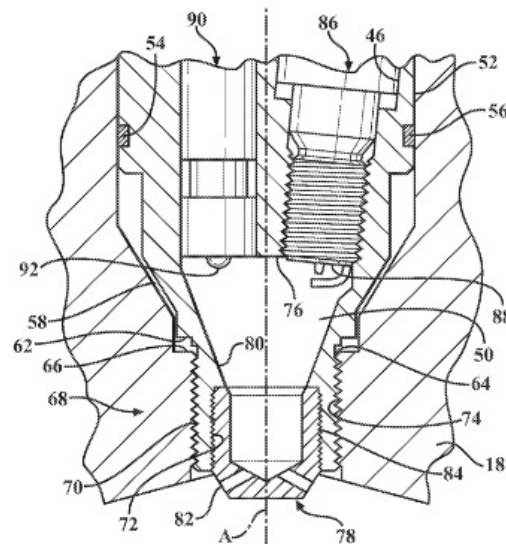


Figure 2.4: Detailed cross-section of TJI system [2]

duced by Mahle GmbH. This scavenged pre-chamber module replaces a spark plug at its place with no extra changes of the engine design. Actually, it is a bi-fuel engine because it has two different supply of an energy. Inside the pre-chamber housing is a spark plug and a gas supply. The gas is directly injected to the pre-chamber. Volume of the chamber is $1,3 \text{ cm}^3$ which is approximately 2% of the compression volume. The second injector is a standard gasoline Port Fuel Injection (PFI) system mounted in an intake manifold and delivers the rest 98 % of an energy. The experimental engine is a single cylinder with four valves. The engine works with a compression ratio of 10,4 and a peak indicated net thermal efficiency of 42 % with almost zero NO_x emissions. Overall swept volume is $0,6 \text{ dm}^3$, the pre-chamber has

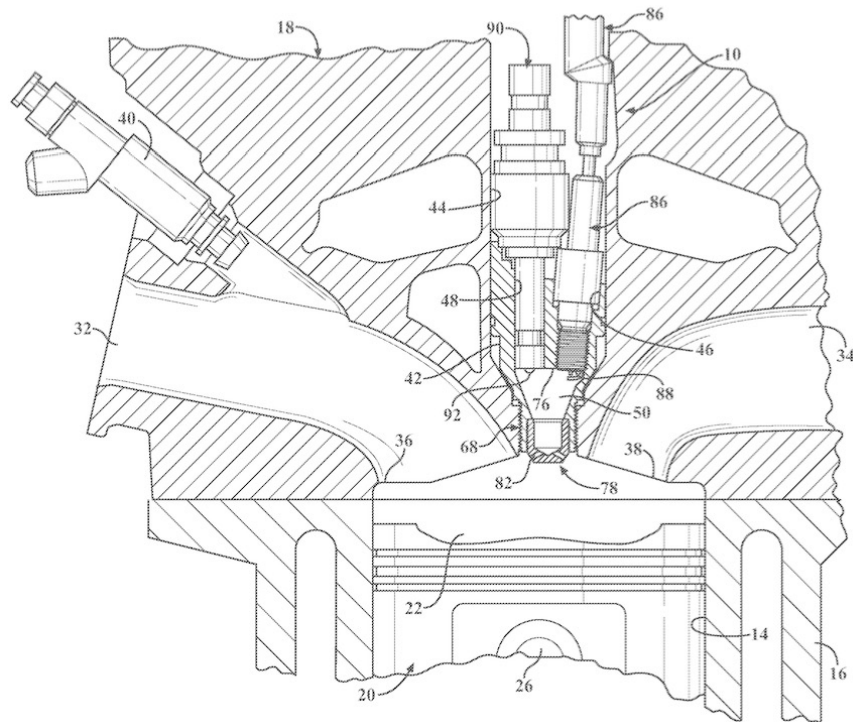


Figure 2.5: Partial cross-section of TJI system [2]

6 holes each with a diameter of 1,25 mm and a length of 3 mm. The relatively small size of orifices causes that the burning mixture travels quickly through the orifices. The pre-chamber combustion products entrain and ignite the main chamber charge through chemical, thermal, and turbulence effects some distance away from the pre-chamber (50) thus producing a distributed ignition system. All together gives a 30 % lower fuel consumption compared to the baseline conventional spark ignition engine. The pre-chamber combustion products entrain and ignite the main chamber charge through chemical, thermal, and turbulence effects some distance away from the pre-chamber (50) thus producing a distributed ignition system. All together gives a 30 % lower fuel consumption compared to the baseline conventional spark ignition engine [2].

The figure 2.5 shows a partial cross-section side view of an engine block (16), a cylinder head (18), a fuel injector (40) and the TJI system (10) mounted in the

internal combustion engine having at least one combustion chamber (22) formed by a piston (20) disposed in a cylinder (14) and enclosed by a cylinder head. A piston pin (26) is there to secure the position with a connecting rod. The cylinder head defines an intake manifold (32) with an intake port (36) and an exhaust manifold (34) with an exhaust port (38). In addition, the cylinder head also includes a fuel

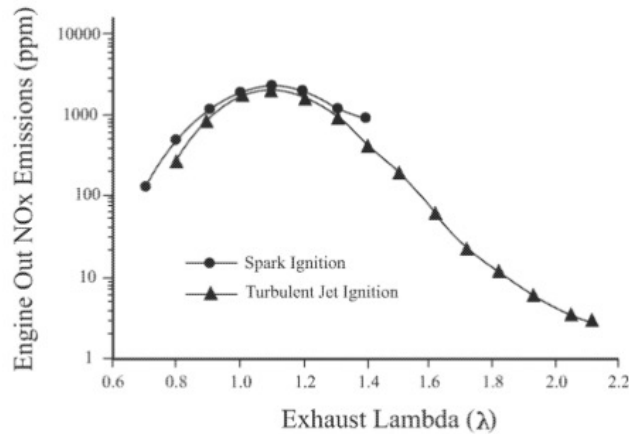


Figure 2.6: NOx comparison of TJI and conventional SI engine [2]

injector mounted in the intake manifold to deliver the main portion of fuel and the port (44) where the whole pre-chamber system (50) is installed. In the figure 2.4 is a detail of the TJI system. The ignition system (86) consists of a housing which gets a support in the port of the cylinder head (18). The housing is a quite complicated part including many surfaces and tunnels to place a spark plug, an injector, a pre-chamber, nozzles and orifices. An o-ring groove (56) is adapted for sealing engagement with the cylinder head. A sealing washer (66) is here to prevent leakages from the combustion chamber. The pre-chamber nozzle (78) includes a few orifices (82) disposed spaced from one another and allow the fuel flows between the pre-chamber (50) and the combustion chamber. The injector (90) has a nozzle (92) that substantially faces the pre-chamber [2].

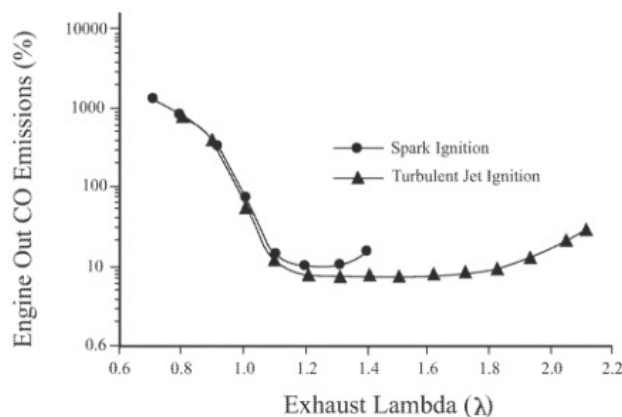


Figure 2.7: CO comparison of TJI and conventional SI engine [2]

An advantage of this ignition system is that it can work sufficiently with a very lean mixture of up to $\lambda = 2,1$ compared to common spark ignition engines which operate up to $\lambda = 1,6$ but usually around stoichiometric value $\lambda = 1$. In figures below are visible differences of CO , HC and NO_x emissions between common spark ignition engine and the scavenged pre-chamber TJI engine. The high level of excess

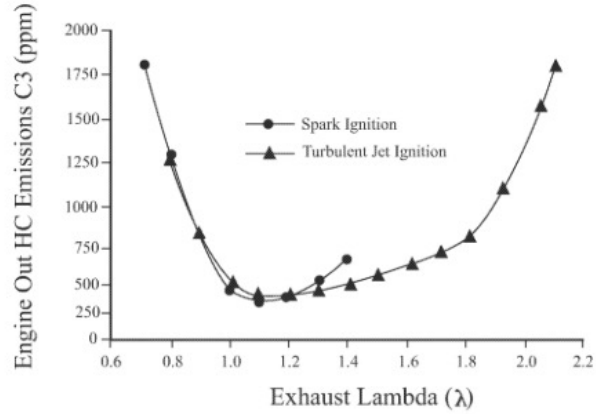


Figure 2.8: HC comparison of TJI and conventional SI engine [2]

air facilitates a very low emissions of NO_x (less than 10 PPM) due to the lower peak combustion temperatures. Figures 2.7, 2.8 and 2.6 show the comparison of conventional spark ignition engine and gas engine with indirect injection. The greatest benefit is obviously in amount of NO_x emissions at lean regime but not only NO_x , the reduction of unburned hydrocarbons and carbon monoxide is also significant.

2.2.2 MWM GmbH

MWM GmbH introduced a patent of a pre-chamber ignition system in 2014. The speciality of the pre-chamber system by MWM GmbH is replacing of a standard spark plug in a cylinder head by the pre-chamber system without any modification.

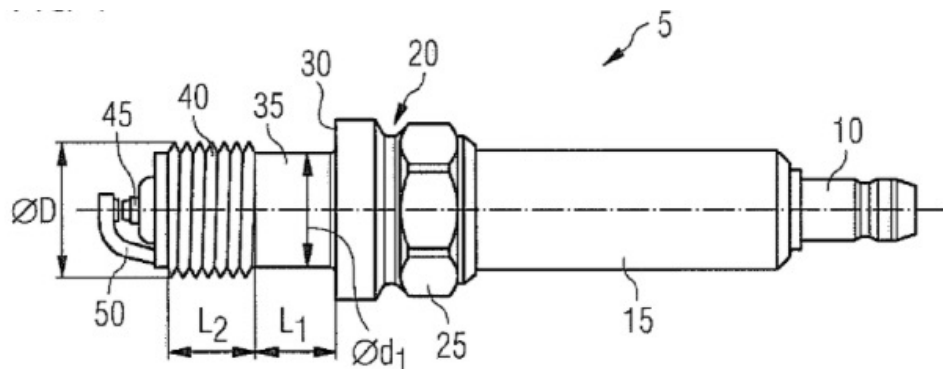


Figure 2.9: MWM GmbH spark plug [12]

It means that at the same prepared internal thread in a cylinder head can be a spark plug or a pre-chamber system. The thread diameter is ranging between M14 and M30. The pre-chamber surrounds a spark plug. This type of a spark plug may be adapted to burn a natural gas, a shale gas, a mine gas, a biogas, a landfill gas or a sewage gas. Fuel has to be pushed by a piston movement into the pre-chamber

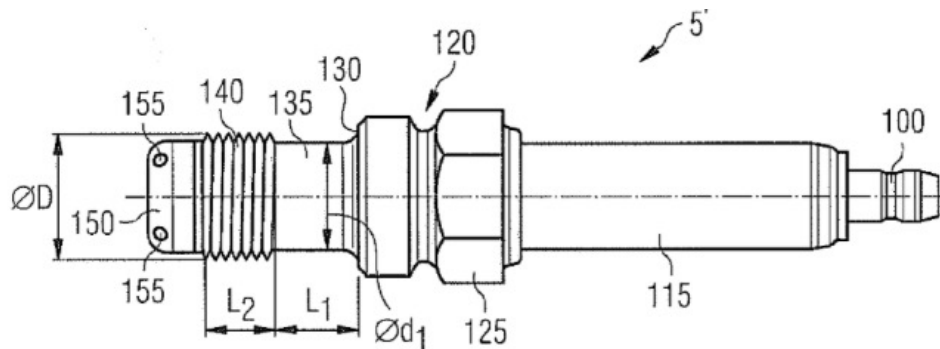


Figure 2.10: MWM GmbH pre-chamber system [12]

because here is no fuel supply inside the pre-chamber which is the main difference compared to other systems. Spark plug then ignites a mixture and the burning mixture enters the main combustion chamber. Figure 2.9 shows a spark plug (5) with a high voltage connector (10), a ceramic insulator (15), an electrode (45) and a ground electrode (50). The shell (20) has a hexagonal section (25) for a wrench and seal face (30). An external thread (40) is screwed into the internal thread in the cylinder head, same for both variants. The intermediate part (35) is without a thread. Figure 2.10 shows the same spark plug but with a chamber (150). Pre-chamber is welded to the spark plug, hence the part is dissembled. This chamber has one or more orifices (155) connecting the chamber with a main combustion chamber [12].

2.2.3 CKD

In the early nineties, Libor Soucek, student of CTU in cooperation with the company CKD was working on the stationary industrial gas engine type 27.5 B8G with indirect injection. Depends on configuration, power output is 1 320 kW for 6 cylinder in-line configuration up to 3 520 kW for 16 cylinder V-engine configuration. BMEP is 1.8 MPa and the maximum of combustion pressure 13 MPa. The figure 2.11 shows detail of the design. The hole in the original cylinder head had to be increased to be possible to implement the pre-chamber system. The new diameter of the hole is 72 mm. This system has its own fuel supply directly into the pre-chamber. Gas is supplied through nine channels with a diameter of 1 mm around the spark plug to achieve sufficiently rich mixture near the spark plug. The pre-chamber is connected to the body of the holder by a union nut. Three holes are drilled in the pre-chamber to connect this volume with the main combustion chamber. Based on the calculation, the top of pre-chamber is under high thermal load and a risk of self-ignition at hot spots is high. The pre-chamber system uses its own recirculation

of cooling liquid as a separated part welded to the pre-chamber body. The volume of the pre-chamber is approximately 2 % of whole compression volume. [19]

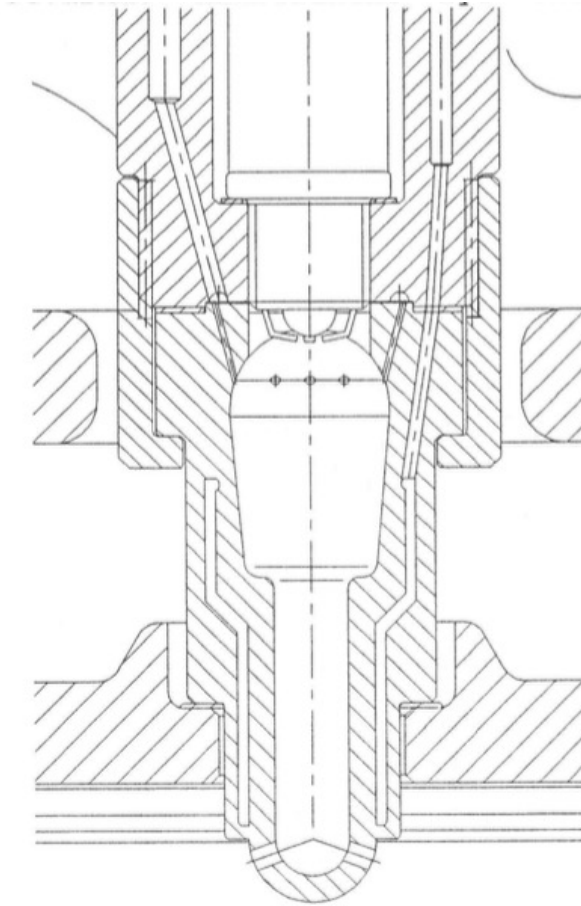


Figure 2.11: Detail of the CKD design [19]

2.2.4 GE Jenbacher GmbH

GE Jenbacher GmbH pre-chamber ignition system is used in a huge stationary engines. A fuel injector is inside the pre-chamber similarly to the Mahle design. In the scavenged pre-chamber, a specific gas quantity is metered into the pre-chamber during an intake and compression stroke via a valve. At the same time, a mixture of air diluted by EGR gasses is introduced to the main combustion chamber via inlet valve. An enriched mixture is ignited inside the pre-chamber which is connected with the main combustion chamber via orifices. The combustion propagates out of the pre-chamber via orifices into the main combustion chamber and there ignites the lean mixture. The figure 2.12 shows a pre-chamber system mounted in a cylinder head (11). The fuel injector (1) fills the plenum (2) and the pre-chamber (10) drilled in the body (8) through channel (3). The fuel is injected to the close surrounding of

the spark plug (12). The shape of the pre-chamber tapers in a direction to overflow channel (4) where the velocity of the flow rises during a compression stroke. The pressure increment scavenges the channel and mixes an enriched mixture inside the pre-chamber with a lean mixture in the main combustion chamber. [5]

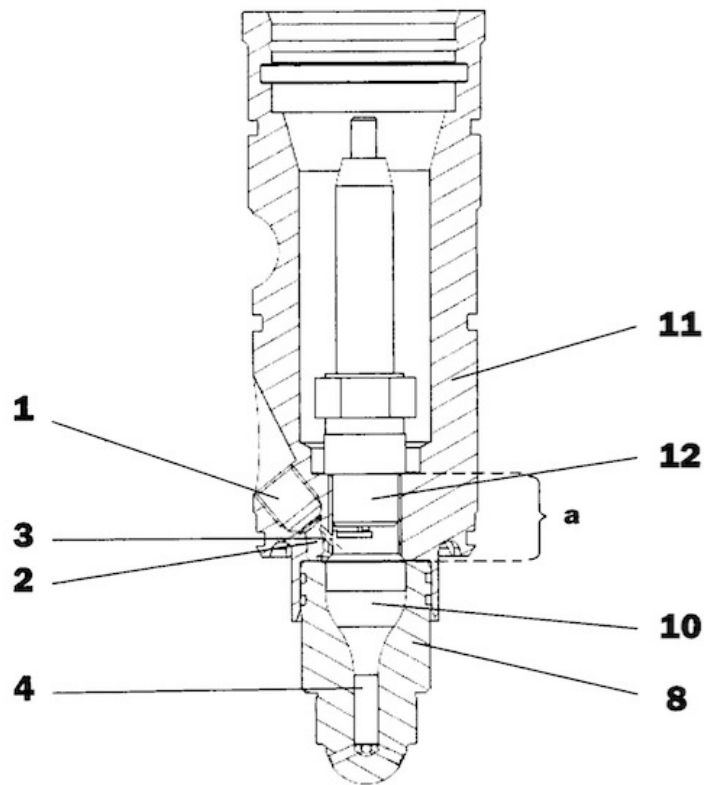


Figure 2.12: GE Jenbacher GmbH [5]

2.3 Daewoo-Avia D432 Engine

All following chapters and my own design is based on this engine which is already mounted at CTU lab and it is used by students and researchers. The cylinder head is made from a ductile iron. The diesel engine series D432 has the bore of 102 mm and the stroke of 120 mm. The engine is designed for light-duty trucks. A bigger engine size was chosen because of more available space for a pre-chamber ignition system and a simple maintenance. Daewoo-Avia D432 is a four stroke engine. It has four cylinder in line and it is turbocharged. The air is cooled down in an inter-cooler. Originally it has direct injection of diesel. The power output of an engine is 100 kW and the torque is 580 Nm.

The engine works with the compression ratio of 17,7. All the parameters of the engine are in the table 2.2.

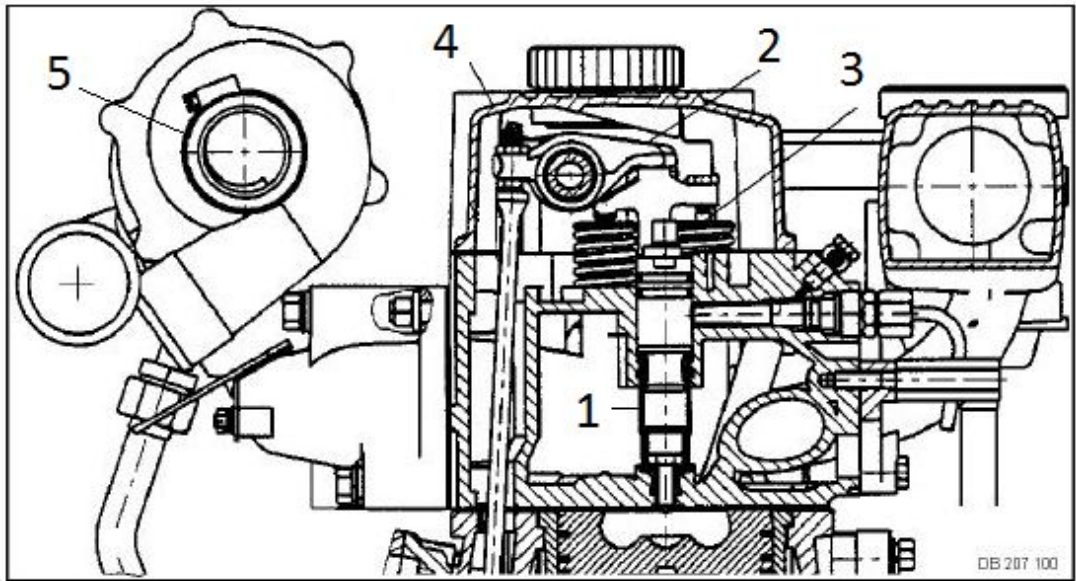


Figure 2.13: Engine Daewoo-Avia [3]

In the figure 2.13 is a cross-section of an original engine D432 and some of its parts: an injector (1), a rocker arm (2) which controls opening and closing of valves (3) and a turbocharger (5) [3].

Type	D432
Principle	4-stroke, diesel
Cylinder	4 in-line
Charging	Turbocharged with inter-cooler
Injection	Direct injection
Swept volume	3 922 cm^3
Bore	102 mm
Stroke	120 mm
Compression ratio	17,5
Power	100 kW/2 400 min^{-1}
Torque	580 Nm/1 200 min^{-1}

Table 2.2: Daewoo-Avia D432 parameters [3]

2.3.1 Engine Modification to SI

The Czech company Tedom a.s. has modified an engine Daewoo-Avia D432 to the stationary spark ignition engine. The fuel is natural gas. In the figure 2.14 is shown an intersection of a cylinder head. The original injector is removed and replaced by a cylinder head housing. In the bottom of a cylinder head is created an internal

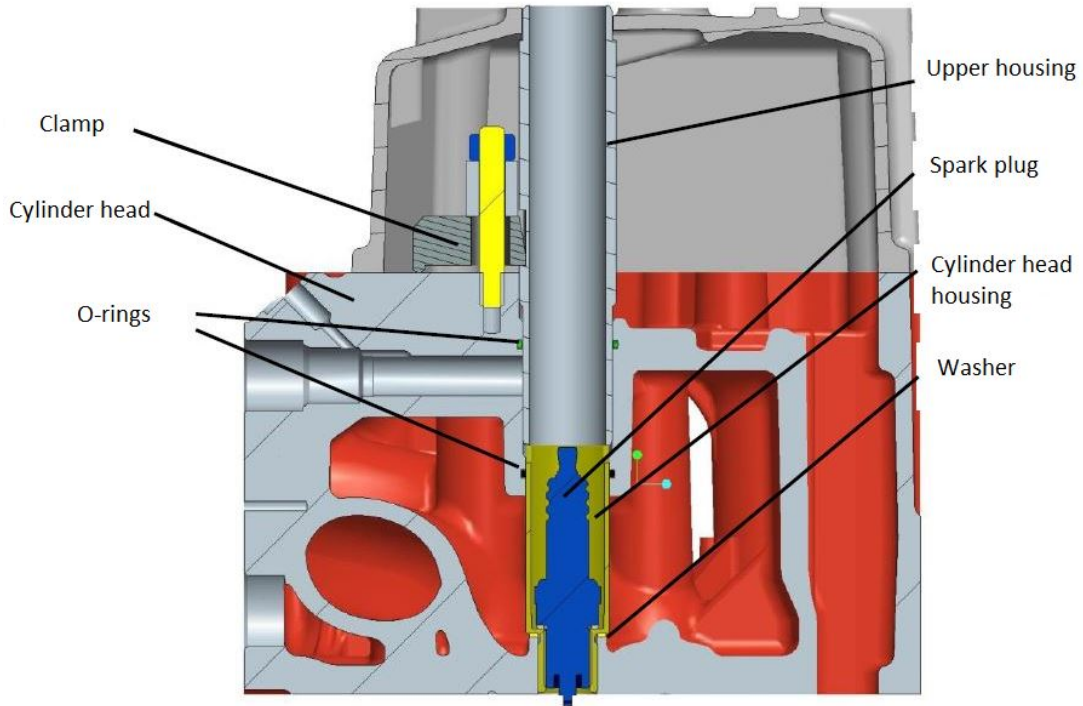


Figure 2.14: Tedom stationary gas engine [21]

thread M18x1. The cylinder head housing protects a spark plug from a cooling liquid. The sealing is provided by a washer at the bottom part and by o-rings at the upper part. The housing has an external thread M18x1 and an internal thread M14x1. The external thread is screwed into the cylinder head and the spark plug is screwed into the internal thread of the housing. The spark plug M14x1 is in the central position in the axis of the cylinder. The upper housing protects spark plug and its electric accessories from the oil. The upper housing has a milled surface where the clamp is mounted and provides a sufficient vertical force against opposite force created by a combustion pressure to hold whole module at the right place. The fuel injector has been moved to intake manifold [21].

2.3.2 Original CTU Scavenged Pre-chamber Design

The idea of the solution is to install a pre-chamber module with a spark plug, a pressure sensor and its own gas supply. The main volume of a gas is injected directly to the surrounding of a spark plug where is enriched mixture easily ignitable and in the main combustion chamber is only a fresh air or very lean mixture given by second

injector, residual or EGR gases. A pre-chamber housing protects a gas pipeline. This solution was designed by my predecessors [21]. Nowadays, it is installed and run

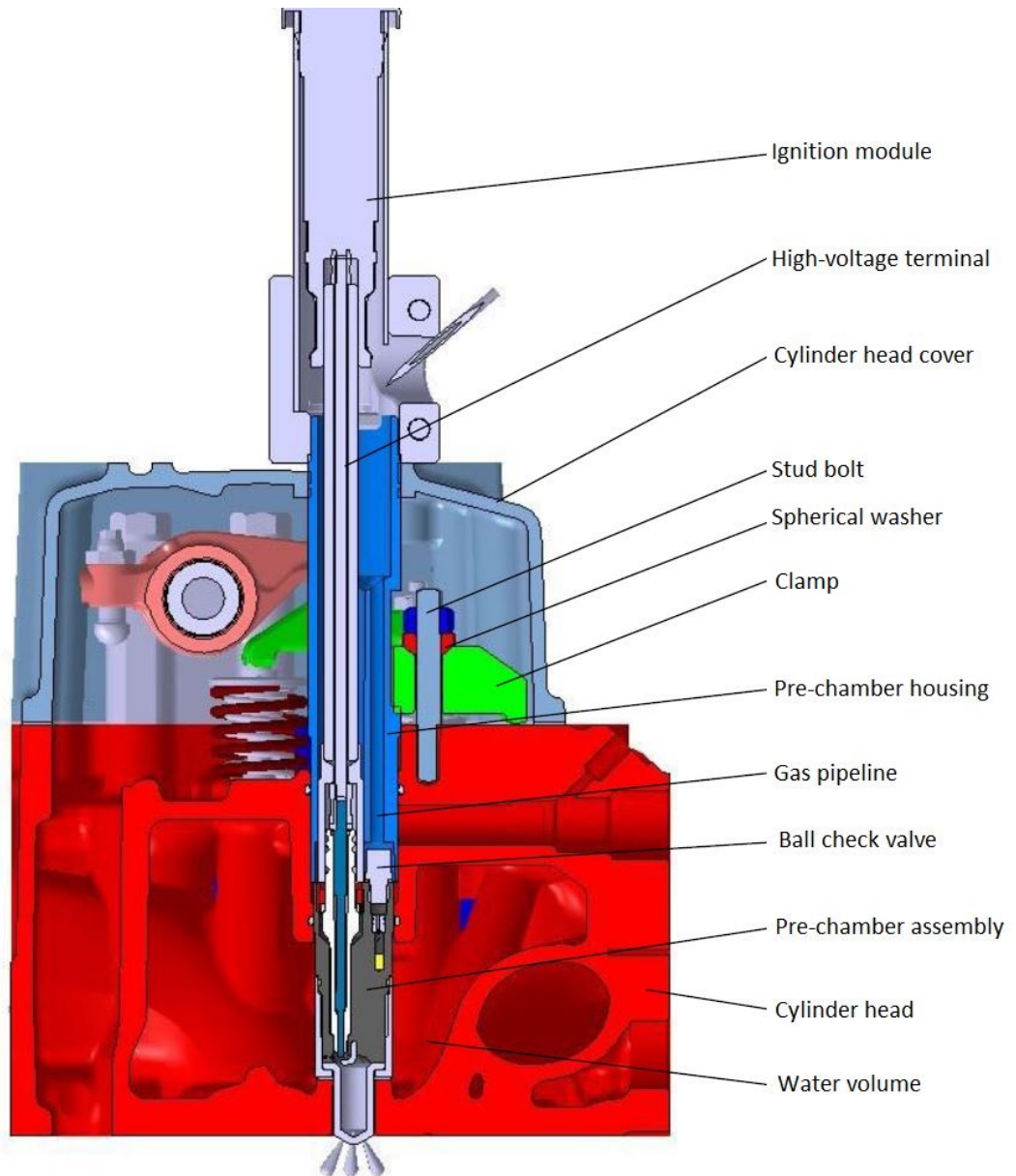


Figure 2.15: The cross-section of the cylinder Head [21]

at the CTU laboratory and a lot of useful data has been acquired. This data is a start point for design improvements of the new generation of a pre-chamber and 3-D CFD model based on the same engine Daewoo-Avia D432. The figure 2.15 shows an intersection of a cylinder head with the most recent design of a pre-chamber module 2.16 system. The ignition module supplies the energy through the high voltage terminal to a spark plug cables and the pressure sensor. The sealing is ensured by an o-ring. The upper part of the module is a quite complicated part which includes a channel for a pressure sensor (not visible), a channel for a gas with a diameter of 1.5 mm, a ball check valve, a fire extinguisher and a space for a spark plug in the

figure 2.17. The chamber is inserted into the union nut, then the copper washer is inserted and finally screwed together with the upper part. The sealing of this part against the cooling liquid is ensured by o-rings and particularly by a thread inside the union nut. The sealing against water in the main combustion chamber is ensured by a washer between the union nut and the cylinder head. To hold the whole module at the right place is solved in the same way like Tedom did by a clamp. To ignite the mixture is used an improved spark plug by a company Brisk Tabor. The improved spark plug is shown in the figure 2.17. The original spark plug has an external thread M10x1. The solution is limited by a limited space and that is why it is not possible to use a complete spark plug, hence only the porcelain part with an electrode was used. The second electrode is welded as a part of a chamber later on after discussion with the spark plug producer. The insulator is put into the

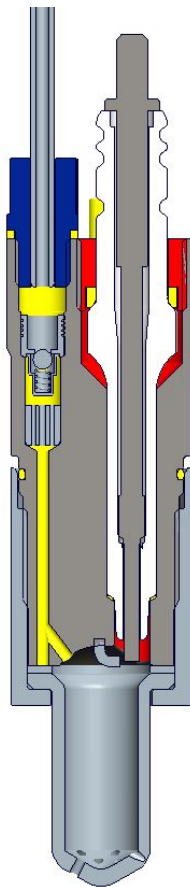


Figure 2.16: Module of a Pre-chamber [21]

channel. The special hollow screw is made to create a sufficient pressure to hold the spark plug at the right place. Natural gas flows through the pipeline. It is necessary to use a miniature check valve which controls a flow of a gas. The ball check valve 558 Series by Lee company was chosen because of a very small dimensions as well as a good material performance and a heat resistance. The gas flow is controlled by pressure differences. The body of a ball is made from a stainless steel same like the ball. The valve is fitted to the upper part and it is not possible to remove it without

total destruction of the valve [21].

The fire extinguisher is installed because of a risk of reverse blast of a flame. An area of the fire extinguisher absorbs an energy from a flame and it is cooled down. It contains 7 channels with a diameter of 0.8 mm. The whole part is 5 mm long and it fits under the check valve. The chamber has a volume of approximately 2 % of a compression volume and it has six orifices 60° apart with a diameter of 1 mm to connect the pre-chamber with the main combustion chamber. It is inserted in the bottom of the cylinder head. The hole in the bottom of the cylinder head has a diameter of 12,5 mm and an inside diameter of the chamber is 9,5 mm. This part

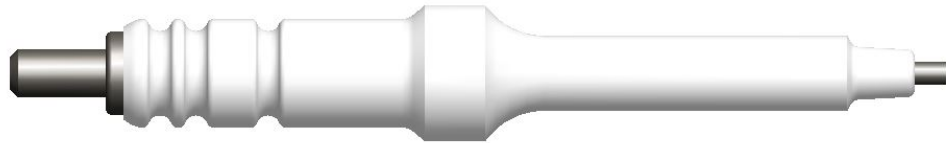


Figure 2.17: The ceramic insulator and the central electrode [21]

has to be made of a material with a high thermal resistivity because the combustion occurs inside. The shape of a pre-chamber is cylindrical. The pressure sensor is used to monitor a pressure inside the pre-chamber. It is possible and very desirable to create an accurate P-V diagram with pressure data connected with a data from the Hall probe which records a position of a crank shaft. AVL GH15D pressure sensor is used. The pressure sensor is not visible in these figures. The channel for this pressure sensor is eccentrically drilled and moreover it is not drilled in the axis of the part [21].

Chapter 3

Design Part

The 3-D CAD model and drawings are created in PTC Creo software. This chapter refers to the drawing documentation in the attachment outside the thesis. In the beginning, there are several requirements which the project has to conform. The main constraint is that the cylinder head is given and it means that the module has to fit to a given size with a minimum changes. The module has to contain a spark plug, a fuel supply and a pressure sensor. The spark plug has to be mounted in the central position and has to be mass produced with no extra adjustments because it is required to switch the engine regime from only one cylinder to all four cylinders and each extra adjustment makes difficulties thus the project is more expensive. There is also a possibility to use a pressure sensor just for one cylinder and this allows to make more simple and cheaper design for the rest three modules. It was decided that the gas supply is guided in an already existing side tunnel which was originally used to fuel supply. A very important requirement is to provide a symmetric distribution of a gas into the combustion chamber. This feature provides a better scavenging around the spark plug.

3.1 Cylinder Head

The engine series D432 of the manufacturer Daewoo-Avia mounted to light-duty trucks is used. The cylinder head is made of a ductile cast iron. The only one change at the cylinder head is that the original hole for fuel injector is increased and grooves for o-rings are re-made. The hole and the position of grooves are visible in the figure 3.2. Now, the hole for the module has a diameter of 29 mm and two 29x1,5 mm o-rings are used. Basic dimensions of the cylinder head, details of the drilled hole and grooves for o-rings are in the drawing number 3-000. The side channel is used for the gas supply, sub-assembly drawing number 4-003-SUBASM. The hole for the chamber in the bottom part of the cylinder head is already re-drilled from originally 7,7 mm to 12,6 mm and the contact surface for the sealing copper washer is machined. This diameter remains. The figure 3.1 shows a space for pre-chamber modules. There are two o-rings, the first prevents the penetration of the oil from the top part to the side tunnel and down to the cooling liquid. The second o-ring

prevents the penetration of cooling liquid from the bottom part. Both o-rings have to withstand high temperature and that is why FPM 80 DIN 3770 o-rings by a manufacturer Rubena a.s which is able to work in a range of $-20\text{ }^{\circ}\text{C}$ up to $+220\text{ }^{\circ}\text{C}$ are selected. This material is suitable to be in the environment of hot water, hot steam or mineral oil [16].

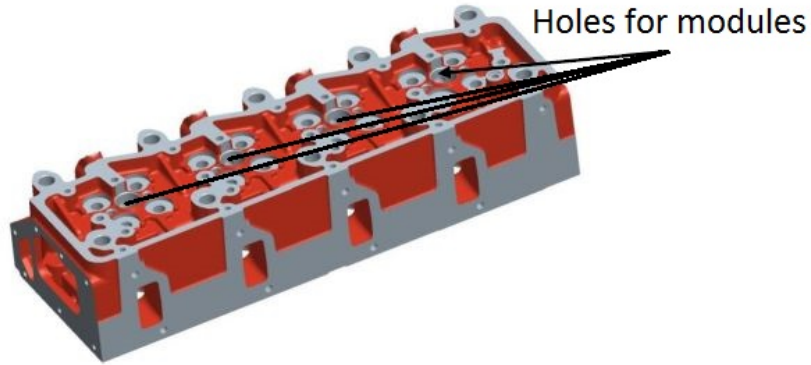


Figure 3.1: Cylinder head of an engine D432 series

Grooves for o-rings are made in the hole based on Rubena a.s recommendation as well. The chamber fits in the cylinder head with a small clearance so that the complete module is possible to remove as a one part with no need of remove the cylinder head. The valve cover remains the same.

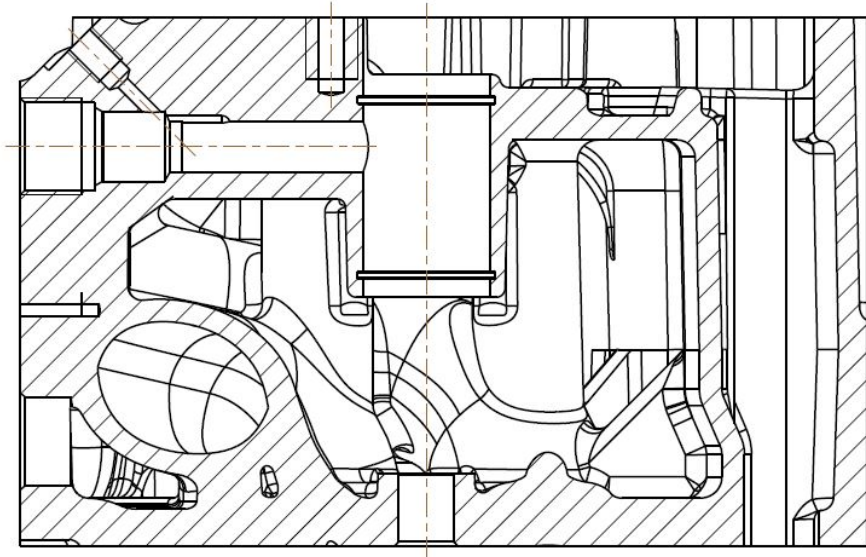


Figure 3.2: Cross-section of an improved cylinder head with o-rings

3.2 Module Housing

The module housing consists of two parts. The chamber, drawing number 3-001, and the covering tube, drawing number 4-002. These two parts are pressed together. The chamber in the figure 3.3 connects main combustion chamber in the piston with the combustion volume in the chamber. The chamber fits with a clearance inside the cylinder head. The connection between the chamber and the cylinder is created by twelve small orifices with diameter of 1,2 mm. These orifices are in two rows 60° apart each other in one row, each row is 30° apart. Inner diameter of 9 mm is created by a drill. The chamber fits with the covering tube with a transition H7/s6

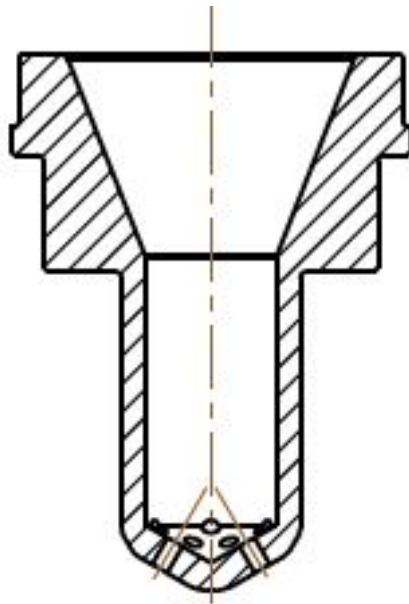


Figure 3.3: Chamber

according to the literature [10]. It provides a sufficient sealing against the cooling liquid. The surface which is in a contact with the spark plug socket is ground. The combustion process releases a huge amount of a heat, hence the material has to be able to withstand a high temperature as well as a high combustion pressure and that is why a chromium-nickel stainless steel 1.4878 is selected. The main characteristics of this material are good corrosion resistance, excellent formability, excellent weldability and excellent impact strength. Detailed information about this material is in a material sheet in attachments.

Based on the figure 3.4, the chamber is divided into a five symmetrical shapes. The volume V_1 is a cone created by a drill.

The vertex angle of the drill is 120° . The volume V_2 is a cylinder created by a body of the drill. V_4 is a cylinder but created by a shape of a copper washer. V_3 as well as V_5 are truncated cones given by machining of each part. It is already known that the combustion volume is approximately 80 mm^3 .

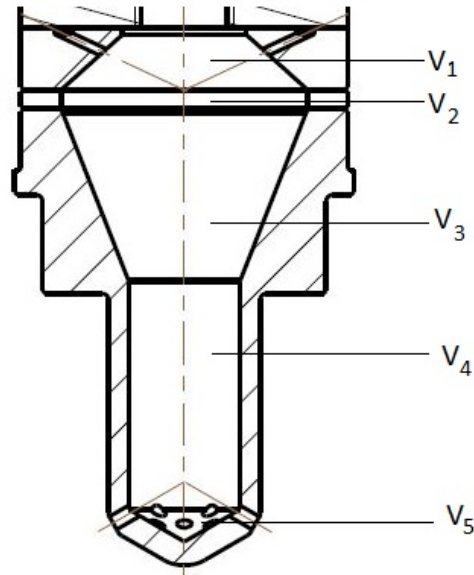


Figure 3.4: Volume of the chamber

$$V_1 = \frac{\pi \cdot r^2 \cdot h}{3} = \frac{\pi \cdot 4,5^2 \cdot 2,6}{3} \cong 55,1 \text{ mm}^3 \quad (3.1)$$

Where:

r...radius of the drill [mm]

h...height of the top of a drill [mm]

$$V_2 = \pi \cdot r^2 \cdot h = \pi \cdot 4,5^2 \cdot 18,5 \cong 1.176,9 \text{ mm}^3 \quad (3.2)$$

Where:

r...radius of the drill [mm]

h...depth of the hole [mm]

$$V_3 = \frac{\pi \cdot h}{3}(r_1^2 + r_1 \cdot r_2 + r_2^2) = \frac{\pi \cdot 14}{3}(4,5^2 + 10 \cdot 4,5 + 10^2) \cong 2.422,7 \text{ mm}^3 \quad (3.3)$$

Where:

h...height of a cone [mm]

r_1 ...radius of the cone base [mm]

r_2 ...top radius of a cone [mm]

$$V_4 = \pi \cdot r^2 \cdot h = \pi \cdot 10^2 \cdot 1,5 \cong 471,2 \text{ mm}^3 \quad (3.4)$$

Where:

r...inside radius of the washer [mm]

h...height of the washer [mm]

$$V_5 = \frac{\pi \cdot h}{3}(r_1^2 + r_1 \cdot r_2 + r_2^2) = \frac{\pi \cdot 4,5}{3}(10^2 + 10 \cdot 5 + 5^2) \cong 824,7 \text{ mm}^3 \quad (3.5)$$

Where:

h...height of the cone [mm]

r₁...radius of the cone base [mm]

r₂...top radius of a cone [mm]

$$V_{Total} = \sum_{n=1}^5 V_i \quad (3.6)$$

$$V_{Total} \cong 55,1 + 1.176,9 + 2.422,7 + 471,2 + 824,7 \cong 4.957 \text{ mm}^3 \quad (3.7)$$

Where:

V_{Total}...Total volume of the chamber [mm³]

$$P_{\%} = \frac{V_{Total}}{V_{Combustion}} \cdot 100 = \frac{4.957}{80} \cdot 100 \cong 6,2 \text{ \%} \quad (3.8)$$

Where:

V_{Total}...Volume of the chamber [mm³]

V_{Combustion}...Overall combustion volume [mm³]

The equation above shows the percentage fraction of the pre-chamber V_{Total} with respect to the overall combustion volume V_{Combustion}. Overall combustion volume is approximately 80 mm³. The result is that about 6,2 % of overall combustion volume consists of the pre-chamber itself. This is a huge progress compared to the original pre-chamber where the percentage fraction is only about 2 %.

The covering tube, drawing number 4-002, has two main functions. The first is to isolate the module from the cooling liquid and second is to hold the module together and allow to manipulate with the module as one part. The tube has an outside diameter of 29 mm and inside diameter of 26,5 mm. The preform is a tube \varnothing 30x2 - 60. The chamber fits in the tube with a transition and all parts inserted to the tube fit with a small clearance. The selected material for the tube is a stainless steel 1.4878. In the upper part of the tube is a hole through the wall for adjusting screws

which are used for holding the module together during putting the module in or out the cylinder head. The hole is bigger than adjusting screws to ensure that the clearance is sufficient and no force is applied by the clamp to the covering tube. The edges of these holes have to be rounded to prevent a destruction of an o-ring during installation of the module. When the tube is cut, chamfer is machined, holes are drilled and rounded. Hot pressing method is used to insert the chamber to the tube. The chamber is cooled down and the covering tube is heated up before the pressing. The figure 3.5 shows the final module housing, drawing number 4-006-SUBASM.

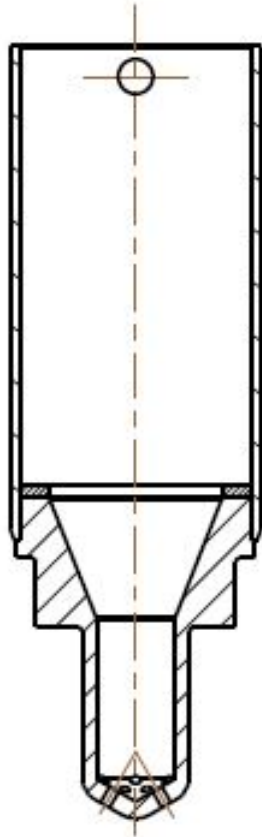


Figure 3.5: Module housing

3.3 Spark Plug Socket

The spark plug socket, drawing number 3-003, is definitely the most complicated part of the module. This part in the end contains many other parts like a ball check valve, a pressure transducer and even it provides a symmetrical distribution of the gas.

The weldment itself consists of two parts - bottom, drawing number 3-017, and top, drawing number 4-016. Preform is a stainless steel rod for both parts. The material is same 1.4878 stainless steel like for the chamber and covering tube. It has

to withstand a high pressure as well as a very high temperature. This part is very small and that is why the laser welding method with no additional material was chosen. This method is fast, doesn't cause a big deformation of the the part. The principle of the laser welding is that the parallel beam from the laser is focused to the chosen point using an appropriate optics. Due to the high energy concentration is the heating rate orders of magnitude higher than the energy dissipation. Requierements for succesfull laser welding are the perpendicular direction of the laser beam to the welded surface, the constant distance and velocity from the welded surface and a protection of the optics. [11]



Figure 3.6: Weldment preform - bottom part

The channel which allows a symmetrical distribution of the gas into the chamber is a reason why two parts are used. The purpose of a symmetrical distribution of the gas is to achieve a better scavenging. The figure 3.6 shows the shape of the channel, a position of two holes for pins and a hole for a spark plug. The channel is created in the bottom part by a milling machine perpendicular to the the hole in the top part. Two pins are here to hold a position of these two parts before both parts are welded together and become a one part. These two holes have a diameter of 1,5 mm and they are 2 mm deep. Last operation with this preform is that the truncated cone is machined. There has to be a space for one more weld around the edge from the bottom side. This weld seals the chamber.

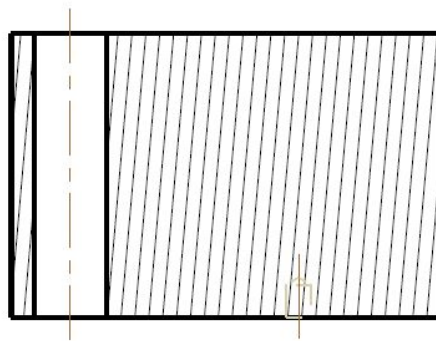


Figure 3.7: Weldment preform - top part

The top part in the figure 3.7 as a preform is a simple cut rod with a hole through. It has a length of 17,5 mm, the diameter of 26,5 mm. Into this part is drilled a hole where the gas flows and two holes for pins to hold the positions with the bottom part.

The figure 3.8 shows the final product. The top and the bottom parts are welded together, a surface and a groove are milled to make a space for the Optrand pressure transducer. The edge has to be also welded to avoid leakages. Then the thread M3x0.5 is drilled through the bottom part. The thread has to be through the material because the sensor processes the pressure during combustion. The thread M8x1 for the spark plug is drilled along the middle axis. The last hole is particularly prepared hole from the weldment preform. The hole for the Lee ball check valve has to be created very accurately. Below the valve is still a space for bronze wool and the pad. At the top side are drilled two holes for pins.

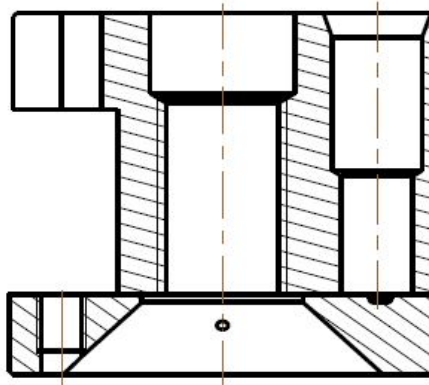


Figure 3.8: Spark plug socket

3.4 Insertion

The function of the insertion, drawing number 4-004, is to provide a sufficient area to transfer a force created by the clamp to the bottom of the module. The preform for this part is a steel rod $\varnothing 30 - 20$ CSN 42 5510.12. The diameter of the final

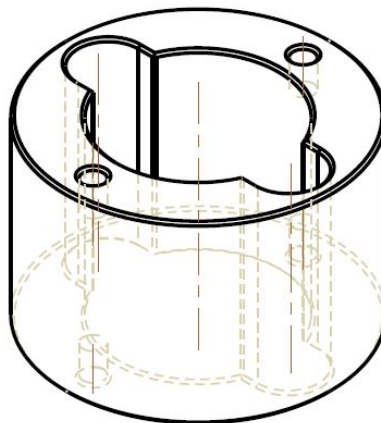


Figure 3.9: Insertion

product is 26,5 mm and the length is 17,5 mm. The selected material is a steel 1.0070. This selected material does not have to withstand a high temperature, it is not welded and the composition with all features of this structural steel is in the material sheet in attachments. The hole with a diameter of 16 mm is for a spark plug, two symmetrical grooves with a radius of 3 mm for a gas tube and a pressure sensor cable and four 3 mm deep holes with a diameter of 2 mm for pins. At each side are two holes. Both faces are ground. The insertion 3.9 is completely symmetrical.

3.5 Gas Elbow

The main functions of the gas elbow, drawing number 3-007, in the figure 3.10 are changing the flow direction of the gas from the side tunnel to the chamber and transferring the force from the clamp to the bottom part of the module. The preform is a steel 1.0070 rod with a diameter of 30 mm. In the middle is a hole for the spark plug cables and Teflon tubes. The second hole is throughout the material and it has a diameter of 4,1 mm. It is for a pressure sensor cable. Two 3 mm deep holes with a diameter of 1,5 mm are drilled at the bottom face. At the place of connection

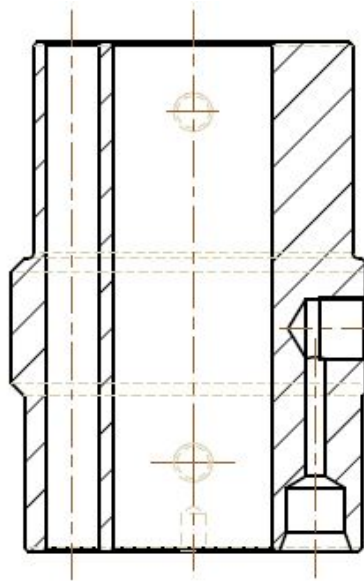


Figure 3.10: Gas elbow

with the gas tube from the side tunnel is milled a surface and perpendicular to the surface is drilled a thread M3x0,5. The surface here is a contact surface between the gas elbow and the washer to provide sufficient area for sealing leakages of a gas. At a bottom face is a 5 mm deep drilled hole with a diameter of 4,6 mm for a gas tube. This hole continues by smaller 17 mm long hole with a diameter of 1,5 mm. Around the bottom edge is machined a chamfer 1,5x20 ° to ensure the o-ring is not destroyed while installation. There are also four threads M3x0,5 for adjusting screws positioned on the side.

3.6 Upper Housing

The upper housing, drawing number 3-008, is situated in oil and air environment and that is why a steel 1.0070 is selected. Preform is a 150 mm long rod with a diameter of 30 mm. It has to transfer the force from the clamp. The force hold the module at the right place. Through the upper housing are driller two holes. First of them is in the middle with a diameter of 12,5 mm for the ignition system accessories and the second hole with a diameter of 5 mm is for the pressure transducer cable. In

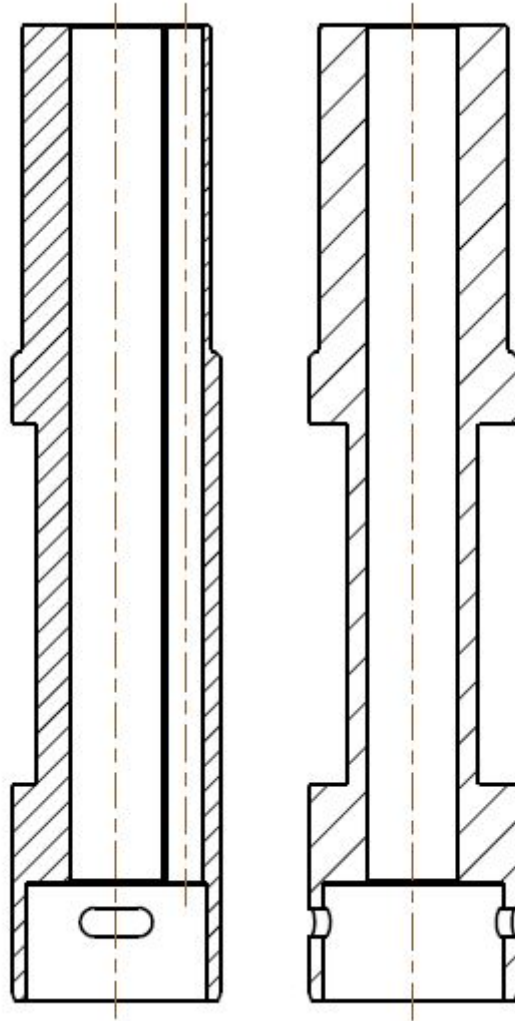


Figure 3.11: Upper housing

the bottom part is a hole with a diameter of 25 mm where is inserted the gas elbow. Adjusting screws are used to hold these two parts together. Threads for adjusting screws are in the gas elbow and in the upper housing is only a hole on the side. The hole has an elliptical shape because the clamp is not in the same plane thus it has to be possible to rotate with the upper housing in a range of few degrees.

3.7 Purchased parts

From the point of view of total costs, it is very important to use as much mass produced parts as possible. Purchased parts are a cylinder head, a spark plug, o-rings, washers, a pressure transducer Optrand, a ball check valve Lee, pins, adjusting screws and a bronze wool.



Figure 3.12: Bronze wool

There are two o-rings in the cylinder head, the first prevents the penetration of the oil from the top part to the side channel and down to the cooling liquid volume. The second o-ring prevents the penetration of the cooling liquid to the bottom part. Both o-rings have to resist a high temperature and that is why FPM80 DIN3770 material is chosen. The material is able to work in a range of $-20\text{ }^{\circ}\text{C}$ up to $+200\text{ }^{\circ}\text{C}$. Another o-rings seal the gas leakages from the gas tube sub-assembly 4-004-SUBASM. The material is same. The last o-ring is in the bushing at the top. The bronze wool has a function of a flame extinguisher. It reduces the heat stress of the ball check valve. The same material is used as an accessory for the welding hoses.

3.7.1 Spark Plug

The implementation of the original spark plug is a huge progress and it was one of the most important task. The smallest mass produced spark plug NGK M8x1 in the figure 3.13 is used. The spark plug is originally from a motorbikes. Unfortunately



Figure 3.13: Spark plug NGK ER8EXIX M8x1

the original termination is too big to use it that is why the reduction from last generations is used. It means the wire with the spark plug terminations, drawing number 4-008, is used and the wire is inside two Teflon tubes DN6 and DN10. Teflon tubes isolate the wire. The sealing of the spark plug provides a contact surface between the spark plug socket and the washer at the spark plug. In the next optimisation it is possible to create a bigger hole and shorter thread in the spark plug socket to move the spark plug deeper inside the chamber.

3.7.2 Miniature Pressure Transducer

The pressure transducer inside the combustion volume together with the Hall probe at the flywheel gives a very useful information about the pressure with respect to the crank angle. They are ideal for a number of applications at the internal combustion engine, for example: engine calibrations (mapping), engine knocking studies and a peak pressure measurement. It is possible to create a BMEP diagram, compare cycle

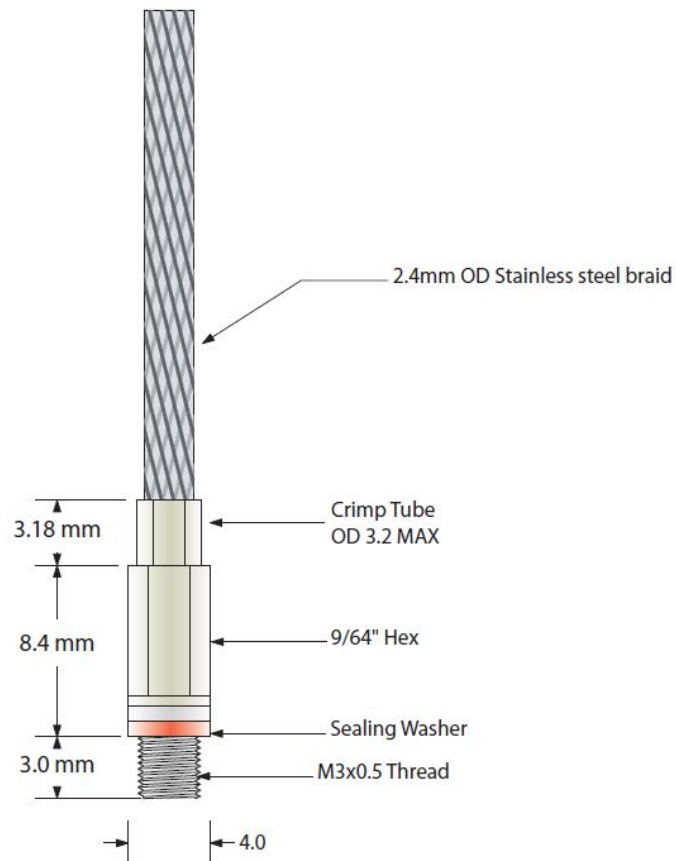


Figure 3.14: Optrand M3x0.5 pressure transducer

to cycle variations or tuning the design to achieve a better solution. The installation of the pressure transducer is the only possibility how to get experimental data for investigation of processes inside the pre-chamber. These data are used for validation

and calibration of 3-D CFD model. For our case it is necessary to use a miniature pressure transducer which is mounted next to the spark plug. Conditions for the sensor is to withstand a high pressure and the high temperature. In this case Optrand M3x0,5 pressure transducer is used. The sealed-gauge sensors utilize multiple optical fibres positioned in front of a flexing metal diaphragm. The intensity of the reflected light is proportional to the pressure induced deflections of the diaphragm. Other option was to buy a kit where the pressure sensor is mounted directly with the spark plug. However, this kit is too big to be mounted in this cylinder head or as a part of the spark plug. In the figure 3.14 is an original drawing by Optrand. It is enough to use the sensor only in a one cylinder and save costs. Moreover, not only by missing sensor but other parts would be cheaper to produce. The spark plug socket without sensor would be much simpler because milling process of the surface is not necessary and that is why the weldment is only around the cylindrical shape of the socket. Next cheaper part is the upper housing where is no more necessary to drill two holes and the part is symmetrical and even more cheaper to produce. An official drawing from the catalogue is in attachments.

3.7.3 Ball Check Valve

Check valves are a mechanical valves that permit a gas to flow in the only one direction, preventing the reverse flow. Check valves are in general very small and inexpensive. Check valves are two-port valves. It means it has one port to entry the gas and one to leave the valve. Fluid flows in the required direction. The ball check valve contains a ball sitting freely above the seat. The ball has larger diameter than the seat and the hole through the seat. If the pressure in direction of flow rises, it

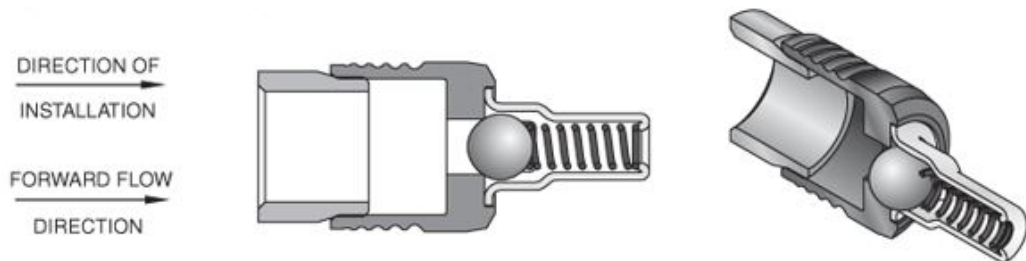


Figure 3.15: Ball check valve LEE 558 series

will push the ball against the spring and it allows the gas flow through the valve. In all other cases the ball is pushed by a spring back to initial position and the ball seals and prevents back-flow of the gas. There is no need to control it manually, it works automatically.

Lee ball check valve 558 series is used. The outside diameter is only 5,6 mm. The valve is pressed into the spark plug socket, where the hole is prepared based on the Lee catalogue. Very important feature of the valve is its cracking pressure. It says what is the minimal generated pressure to push the ball against the spring. The cracking pressure depends on used spring. All the dimensions and used material at this Lee check valve are in the product data sheet in attachments.

3.8 Complete Assembly

All necessary parts are introduced and in this last part is described how to assemble them all together step by step:

1) The spark plug socket 3-003 is assembled with all its accessories. Approximately 2 mm thick layer of the bronze wool is inserted into the side hole where is visible the channel for a gas. The pad, drawing number 4-006, is inserted above the bronze wool. The ball check valve is pressed above both the wool and the pad. The spark plug NGK ER8EXIX is then screwed to the thread in the middle and the pressure sensor Optrand is screwed to the thread M3x0,5 at a side. In the figure 3.16 is visible the first step. The spark plug termination 4-009 is screwed to the thread at the top



Figure 3.16: Step by step assembly

of the spark plug with a wire which is isolated by two Teflon tubes DN6 and DN10. It is used because the original spark plug termination is too big to mount it in.

2) The washer 26x20x1,5 ISO 7089-3 is inserted into the module housing 4-006-SUBASM and then the spark plug socket is inserted. Four pins 2x6 CSN EN ISO 2338 are inserted to the insertion 4-004 as well as a gas tube 4-005 passes through the groove in the insertion. The gas tube 4-005 with two o-rings is inserted to the prepared holes inside the spark plug socket and the insertion. The tube with an



Figure 3.17: Complete module

outside diameter of 6 mm and the wall thickness of 2 mm is purchased from a manufacturer Akros s.r.o. and o-rings 3x1 FPM 80 DIN 3770 and 4x1 FPM90 DIN 3770 are purchased from a manufacturer Rubena a.s. The tube is machined. The gas tube is inserted into the hole above the check valve, the sealing is provided by an

o-ring. The position of the spark plug socket with respect to the insertion is hold by two pins. Second end of the tube is inserted to the hole in the gas elbow 3-007 and position is hold by pins again. To hold the module together, adjusting screws are screwed to the gas elbow. In the housing module is only a hole. The free end of the screws is used while manipulating with the module as a point of contact with the tube. In the figure 3.17 is shown complete module.

3) The upper housing 3-008 is put on the gas elbow. Adjusting screws hold it all together too. Now, the whole module sub-assembly 3-002-SUBASM is inserted into the modified cylinder head 3-000. Sealing is provided by o-rings 29x1,5 FPM80 DIN 37730 inside grooves in the cylinder head.

4) The module sub-assembly has to be turned so that the gas supply sub-assembly 4-003-SUBASM inserted through the side channel is screwed into thread in the gas elbow by a pipe wrench. The gas supply sub-assembly consists of four parts. A gas tube, a Teflon bushing, a tube termination and a washer. The tube, drawing number 4-011, is a product of the producer Akros s.r.o. [1] and the only operation with the tube is to cut to a required length. It has a diameter of 3 mm and the wall thickness of 0,7 mm. The material of the tube is 1.4435. The figure 3.18 shows sub-assembly of a fuel supply which is mounted in the side tunnel. To lead the tube

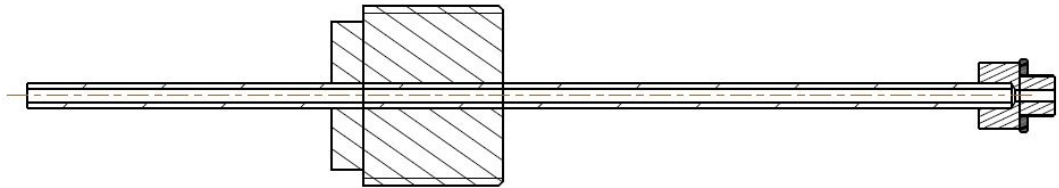


Figure 3.18: Gas supply sub-assembly

and avoid unwanted vibrations a Teflon bushing is used. The material is PTFE and drawing number of this part is 4-010. On the outer diameter is machined a thread M22x1,5. The surface is milled to enable screwing it by a 18 mm wrench key. The same thread is already in the cylinder head.

4) The whole module sub-assembly is then hold at its position by the clamp sub-assembly 4-005-SUBASM. The sub-assembly is situated under the valve cover. The function is to develop a down-force. The shape is defined by the free space between valves. The design of the clamp is from the last iteration. It means that the strength control has been already done [21]. The preform is a square rod and selected material is a steel 1.1191. In case of some deformation of the copper washer or manufacturing inaccuracies the contact surface of the clamp is cylindrical so that the stud bolt is not deformed. The last step is to put the cover of the cylinder head on. A cover and a bushing with an o-ring inside provide the sealing. In the figure 3.19 is shown complete assembly in the cylinder head.

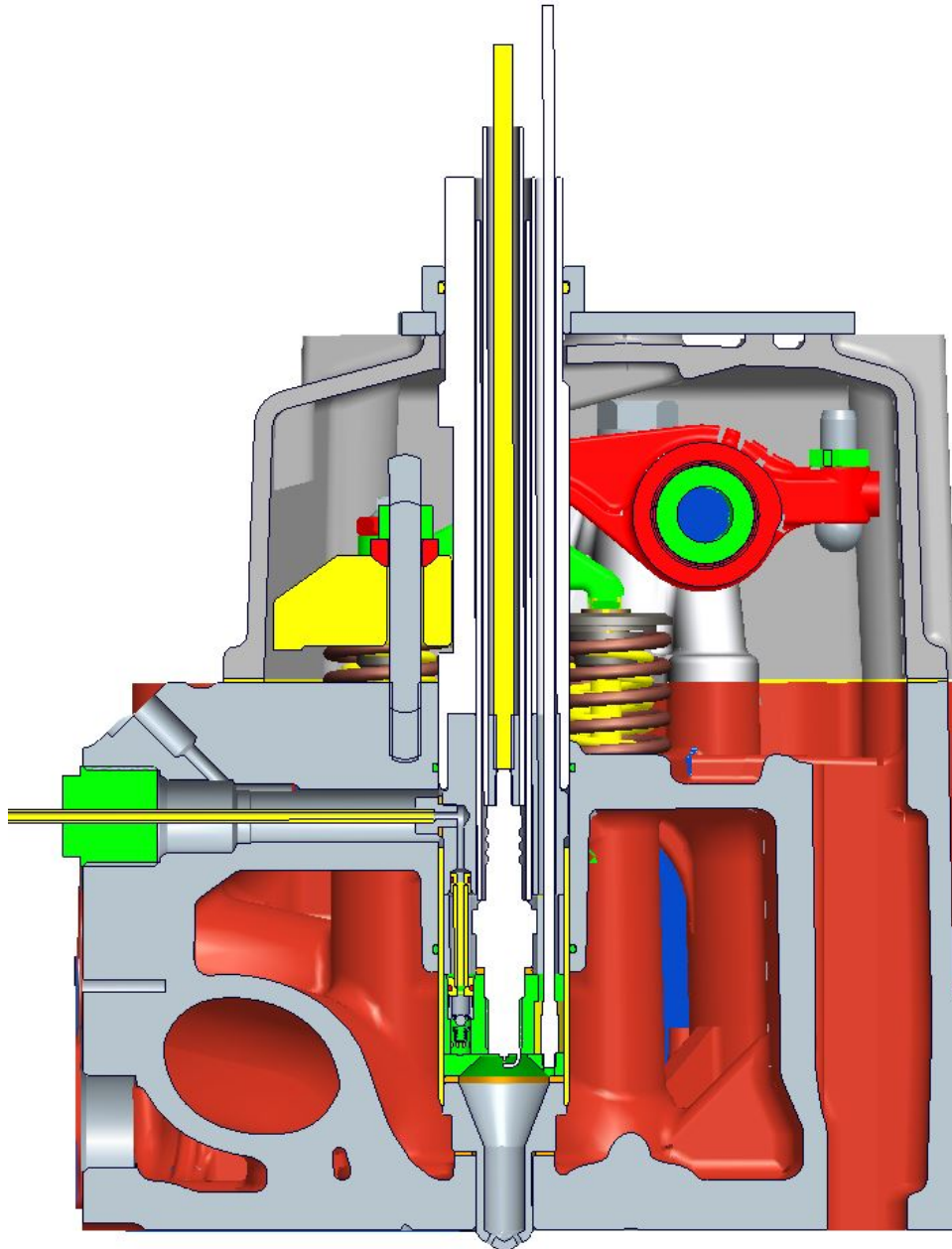


Figure 3.19: Complete assembly

3.9 Version Without the Pressure Transducer

To save costs is appropriate to mount the Optrand pressure transducer to only one module because the sensor itself is very expensive device and one sensor is enough to acquire data. It means that the design of the rest three modules is modified, easier to produce thus cheaper. Especially the spark plug socket where is not a thread for the transducer. The missing transducer causes that it is useless to mill the surface

as well as the groove where the transducer is mounted and the shape is strictly cylindrical. The weld is made all the way round the cylinder. Second weld from the bottom around the inner edge is still the same. Both the top and the bottom preforms remain same but after welding is drilled only a thread for the spark plug and holes for pins. It makes the component much cheaper and easier to produce. The final spark plug socket without transducer, drawing number 3-003-W/O, is shown in the figure 3.20. Preforms for this part remain the same.

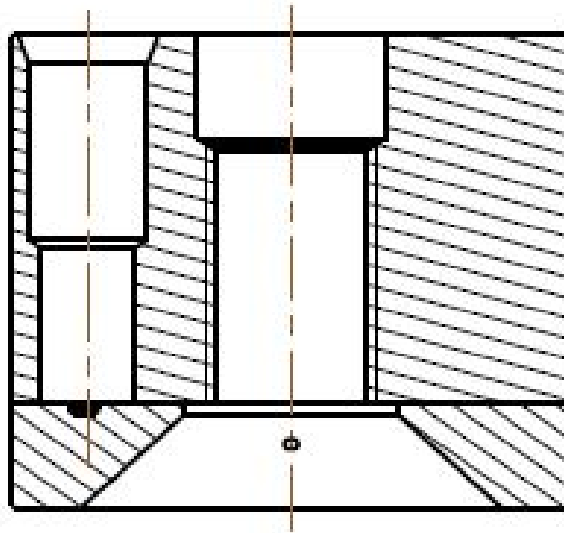


Figure 3.20: Spark plug socket without a pressure transducer

The insertion in the figure 3.21 has only one change. One groove is missing because that groove was originally for the cable of pressure transducer. It cancels one operation at milling machine and creates a larger contact area between the insertion and the spark plug socket at one face and the insertion and the gas elbow on the second face. The drawing number of the insertion is 4-004-W/O. The gas elbow is more modified in a case of missing transducer. Drawing of this part has a number 3-007-W/O. The hole for a cable is missing as well as two threads for adjusting screws at the top side. The top part is completely re-designed. There is a 11 mm long centering cylindrical surface with a diameter of 22 mm continuing by a thread M24x1,5. Adjusting screws are not needed because the connection between the gas elbow and the upper housing provides the thread. Thread for adjusting screws at the bottom side are preserved as well as all other dimensions and features. The gas elbow is shown in the figure 3.22.

The upper housing is also more modified part. The missing hole for a cable allows to make the upper housing completely symmetrical and thus it was possible to create a thread M24x1,5 because now it is possible to rotate with this part to find a right position with respect to the side tunnel in the cylinder head.

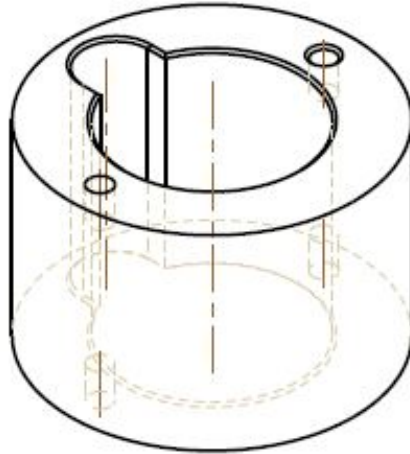


Figure 3.21: Insertion without a pressure transducer

Drawing number of this modified upper housing is 3-008-W/O. The contact surface between the clamp and the upper housing is the same. In the bottom part is a hole and a thread to insert and screw the gas elbow. In the figure 3.23 is the final upper housing. The figure 3.24 shows the complete assembly 3-001-W/O-ASM of the version without a pressure transducer.

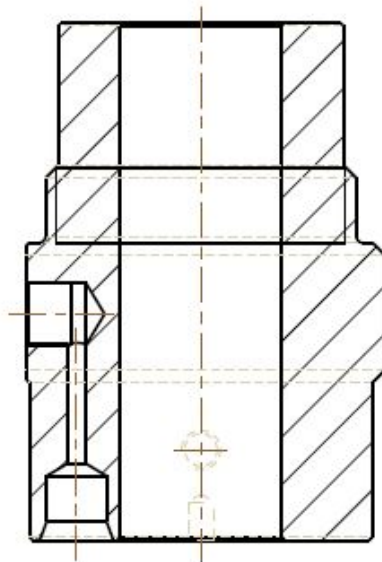


Figure 3.22: Gas Elbow without a pressure transducer

The procedure of an assembly is same like the version with the sensor. The gas supply inside the channel tunnel is without a change as well as the clamp and chamber. The module without the sensor has a drawing number 3-002-W/O-SUBASM.

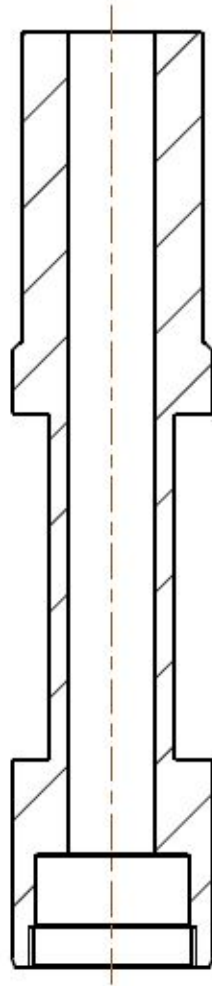


Figure 3.23: Upper housing without a pressure transducer

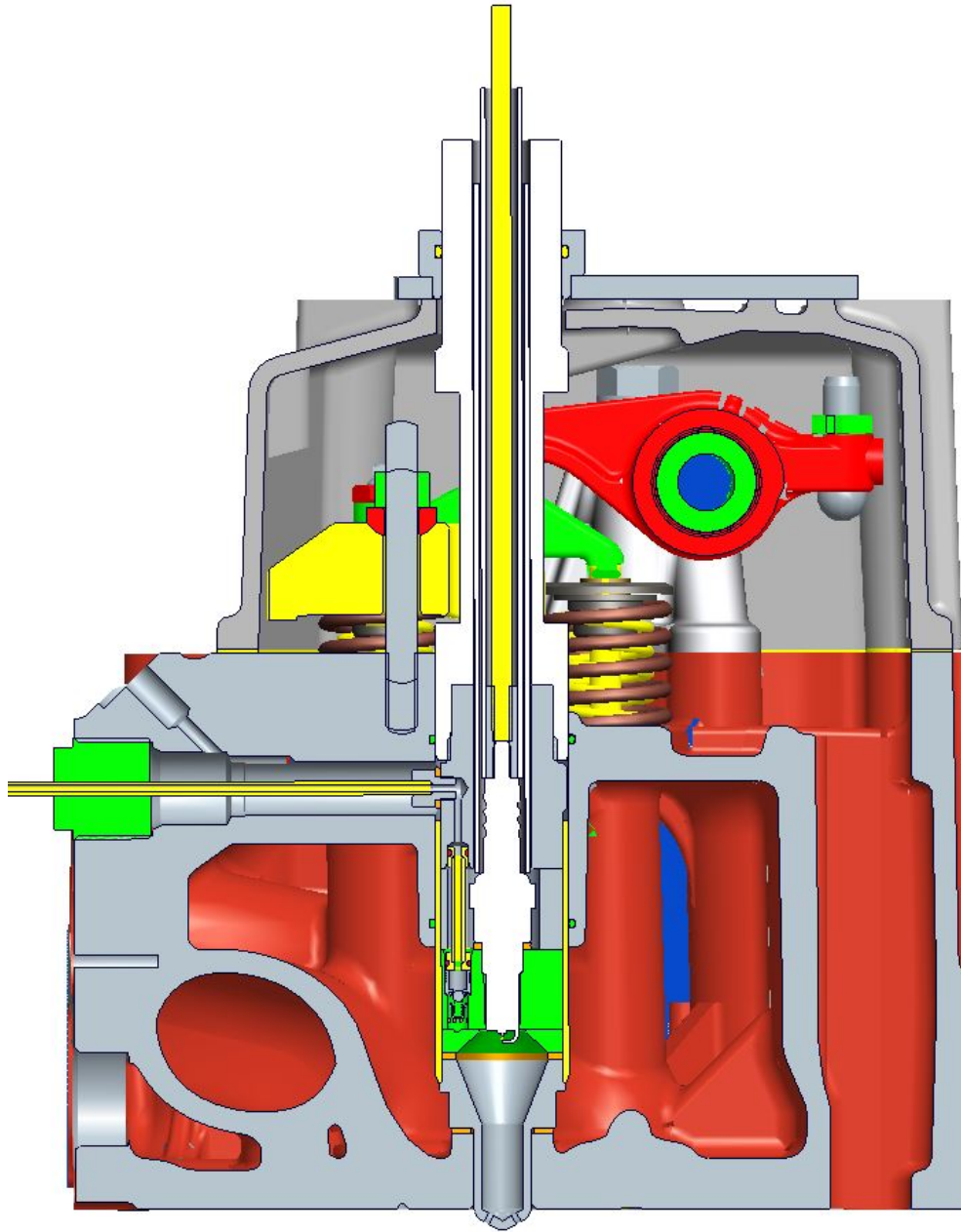


Figure 3.24: Complete Assembly without a pressure transducer

Chapter 4

3-D CFD Part

The 3-D CFD simulation represents the most sophisticated approach for the detailed numerical investigations on the dynamic problems of the fluids. One of reasons why to use 3-D CFD simulation is to understand processes inside the pre-chamber and then modify the design to achieve desired solution. Another very important reason is that the modification based on simulations is much faster and cheaper than the production and experimental testing of prototypes.

The following section describes how the software works. The AVL FIRETM software employs the finite volume discretization model which needs an integral form of the general conservation laws. The flow of a fluid which is a gas or a liquid is governed by the partial differential equations. Partial differential equations represent basic conservation laws for the mass, the momentum and the energy. These three conditions completely cover the behavior of the system. The CFD software solves these partial differential equations by a set of algebraic equations [7].

$$\frac{dm}{dt} = 0 \quad (4.1)$$

The mass conservation law in an integral form 4.2 expresses the fact that mass cannot disappear from the system, nor be created. Mass can be only transported through the convection. The equation of a mass conservation is also called the continuity equation [7].

$$\frac{\partial}{\partial t} \int_V \rho dv = - \oint_S \rho u \cdot nds \quad (4.2)$$

The left side of the equation is the rate of a change of the mass and the right side of the equation is the net inflow of the mass. The negative sign means the inflow. In the other case the negative sign means an outflow, hence the rate of a change of the mass is equal to a net inflow of the mass. The Newton's second law of the motion describes the conservation law for a momentum. The momentum can be changed

by forces acting on the control volume [22].

$$\frac{d(mv)}{dt} = \sum f \quad (4.3)$$

Momentum is a vector defined as a product of a mass and a velocity expressed per unit of a volume.[7] The equation of the momentum conservation law in an integral form:

$$\frac{\partial}{\partial t} \int \rho u dv = - \oint \rho u u \cdot n ds - \oint p n ds + \oint 2\mu D \cdot n ds + \int \rho f dv \quad (4.4)$$

Where the left side of the equation is the rate of a change of the momentum. The right side of the equation contains in the following order the net inflow of the momentum, total pressure, total viscous force and total body force. The surface forces due to pressure and stresses are, from the molecular point of view, the microscopic momentum fluxes across a surface.

The Reynolds number has one of the most important role in the fluid dynamics. It is a non-dimensional ratio between a momentum convection and a diffusion. The higher Reynold's number, the lower influence of friction forces of molecules of the fluid on the overall friction. The flow is turbulent if the Reynold's number exceeds the critical value [22], [4], [7].

$$Re = \frac{uL}{\nu} \quad (4.5)$$

The energy conservation law in an integral form:

$$\begin{aligned} \frac{\partial}{\partial t} \int \rho \left(e + \frac{1}{2} U^2 \right) dv = & - \oint \rho \left(e + \frac{1}{2} U^2 \right) u \cdot n ds + \int_V u \cdot f dv \\ & + \oint n \cdot (uT) ds - \oint n \cdot q ds \end{aligned} \quad (4.6)$$

Where the left side of the equation is the rate of a change of the kinetic and the internal energy. The right hand side of the equation contains in the following order the net inflow of the kinetic and the internal energy, the work done by body forces, the net work done the stress tensor and the net heat flow [22].

The system of Navier-Stokes equations, supplemented by an empirical laws for a dependence of a viscosity and a thermal conductivity with an other flow variables by a constitutive law defining the nature of the fluid, completely describes all the flow phenomena of the Newtonian fluid. For laminar flow it is enough but this model works with turbulent flow, hence the turbulence has ti be introduced. The turbulent flow has some specifics. The turbulent flow is a three dimensional unsteady and

chaotic flow. The turbulence increases the rate at which conserved quantities are stirred, the actual mixing is accomplished by a diffusion. This process is often called a turbulent diffusion. The reduction of the velocity gradients due to the action of a viscosity reduces the kinetic energy of the flow. The lost energy is irreversibly converted into the internal energy of the fluid. An intense mixing is useful when a chemical mixing or a heat transfer are needed. Both of these may be increased by orders of magnitude by the turbulence [4], [7].

There are many models for simulating turbulent flow such as DNS (Direct Numerical Solution), LES (Large Eddy Simulation) or RANS (Reynolds Averaged Navier-Stokes). The *FIRETM* solver uses The RANS model.

The all turbulent quantities a are decomposed into the average and the fluctuation part. The separation is in the following equation.

$$a = \bar{A} + A' \quad (4.7)$$

The symbol \bar{A} is a time averaged turbulent quantity and T is a time which has to be large enough compared to the time scale of the turbulence but still small compared to the time scales of all other unsteady phenomena. The A' is a turbulent fluctuating part which is of the stochastic nature. Pressure and velocity are decomposed according to the equation 4.9 [7].

$$p = \bar{p} + p' \quad (4.8)$$

$$u = \bar{u} + u' \quad (4.9)$$

The time averaging is suitable for the steady turbulent flow.

$$\langle a \rangle = \frac{1}{T} \int_0^T a dt \quad (4.10)$$

The homogeneous turbulent flow is then described by the space averaging.

$$\langle a \rangle = \frac{1}{L} \int_0^L a dx \quad (4.11)$$

The two equation turbulence energy model has to be introduced to understand what equations and models the software uses. In our case, the k- ϵ model is used. It is based on the specific kinetic energy. Specific in this case means that it is a kinetic energy per unit mass.

$$k = \frac{1}{2}(\overline{u'^2} + \overline{v'^2} + \overline{w'^2}) \quad (4.12)$$

Symbols u , v and w are velocity vectors in x , y a z axis. For next step is necessary to introduce the Reynold's stress tensor because the Reynolds stress tensor is proportional to the specific kinetic energy.

$$\tau_{ij} = 2\mu_T S_{ij} - \frac{2}{3}\rho k \delta_{ij} \quad (4.13)$$

For the compressible model after substitution is derived the turbulence kinetic energy equation. This equation is suitable for all energy equation models. The model is suitable for computation of the specific kinetic energy k as well as the turbulent length scale ℓ [24].

$$\rho \frac{\partial k}{\partial t} + \rho U_j \frac{\partial k}{\partial x_j} = \tau_{ij} \frac{\partial U_i}{\partial x_j} - \rho \epsilon + \frac{\partial}{\partial x_j} \left[\left(\mu + \frac{\mu_T}{\sigma_k} \right) \frac{\partial k}{\partial x_j} \right] \quad (4.14)$$

All two equation models start with the Boussinesq approximation, the equation of Reynolds stress tensor 4.13 and the turbulence kinetic energy equation 4.14. The main idea is to derive the exact equation for the dissipation per unit mass ϵ and find other equations governing its behaviour. The ϵ is derived by using the Navier-Stokes equation. 4.14

$$\begin{aligned} \rho \frac{\partial \epsilon}{\partial t} + \rho U_j \frac{\partial \epsilon}{\partial x_j} = & -2\mu \overline{[u'_{i,k} u'_{j,k} + u'_{k,i} u'_{k,j}]} \frac{\partial U_i}{\partial x_j} - 2\mu \overline{u'_k u'_{i,j}} \frac{\partial^2 U_i}{\partial x_k \partial x_j} - 2\mu \overline{u'_{i,k} u'_{i,m} u'_{k,m}} \\ & - 2\mu \nu \overline{u'_{i,km} u'_{i,km}} + \frac{\partial}{\partial x_j} \left[\mu \frac{\partial \epsilon}{\partial x_j} - \overline{\mu u'_j u'_{i,m} u'_{i,m}} - 2\nu \overline{p'_m u'_{j,m}} \right] \end{aligned} \quad (4.15)$$

To describe the right side of the equation the first and the second members are production of dissipation, the third and the fourth members describe the dissipation of dissipation and the last member is the sum of the molecular diffusion of dissipation and the turbulent transport of dissipation. To sum up, the standard k- ϵ model is as follows [24].

Eddy viscosity:

$$\mu_T = \rho C_\mu \frac{k^2}{\epsilon} \quad (4.16)$$

Turbulence kinetic energy:

$$\rho \frac{\partial k}{\partial t} + \rho U_j \frac{\partial k}{\partial x_j} = \tau_{ij} \frac{\partial U_i}{\partial x_j} - \rho \epsilon + \frac{\partial}{\partial x_j} \left[\left(\mu + \frac{\mu_T}{\sigma_k} \right) \frac{\partial k}{\partial x_j} \right] \quad (4.17)$$

Dissipation rate:

$$\rho \frac{\partial \epsilon}{\partial t} + \rho U_j \frac{\partial \epsilon}{\partial x_j} = C_{\epsilon 1} \frac{\epsilon}{k} \tau_{ij} \frac{\partial U_i}{\partial x_j} - C_{\epsilon 2} \rho \frac{\epsilon^2}{k} + \frac{\partial}{\partial x_j} \left[\left(\mu + \frac{\mu_T}{\sigma_\epsilon} \right) \frac{\partial \epsilon}{\partial x_j} \right] \quad (4.18)$$

Turbulent length scale:

$$\ell = \frac{C_\mu k^2}{\epsilon} \quad (4.19)$$

And the closure coefficients:

$$\begin{aligned} C^{\epsilon_1} &= 1,44 \\ C^{\epsilon_2} &= 1,92 \\ C_\mu &= 0,09 \\ \sigma_k &= 1 \\ \sigma_\epsilon &= 1,3 \end{aligned}$$

The CFD modelling is an approximation method and that is why the convergence criteria have to be set. The higher convergence criteria the faster but the less accurate calculation. Deciding when to stop the iterative process on each level is very important, from both the accuracy and the efficiency points of view. The more iteration is set, the more time it consumes but the result is more accurate. A numerical method is said to be convergent if the solution of the discretized equations tends to the exact solution of the differential equation as the grid spacing tends to zero. The convergence is checked using many experiments and experience. The rapid convergence of an iterative method is the key to effectiveness. The iterative method converges if:

$$\lim_{n \rightarrow +\infty} \epsilon^n = 0 \tag{4.20}$$

In an iterative method it is important to be able to estimate the iteration error in order to decide when to stop iterating. The procedure is stopped when the difference is less than the selected value. The closure data for each iteration step is represented by under relaxation factors. An optimum under relaxation factors are problem dependent. A good strategy is to use a small under relaxation factors in the early iterations. The control of the time step is then important in controlling the evolution of the solution [4].

4.1 CFD Model

The aim is to prepare and test a model using the software AVL FIRETM. This section describes the model, its setting step by step and the origin of boundary conditions and initial conditions. The aim of the thesis is not to analyse the data. It is important to emphasize that the simulation does not include the combustion process and it focuses on the quality of a scavenging and leakages of methane during the cycle. All the dimensions and the shape are given by already existing design visible in the figure 2.16. The data for boundary conditions and initial conditions are from 1-D GT-Power model which is validated by an experimental engine and it is the reason why the older design is used. To validate the CFD model was necessary to inject only gas into the pre-chamber and not into the intake manifold. The experiment was specially prepared for validation of the CFD model. In the reality gas is injected to the intake manifold thus inside the cylinder is a mixture of air and gas. The experimental stationary engine is not intended to be a propulsion of the vehicle.

The first step is to import the geometry into AVL FIRE Workflow Manager and set edges and selections. Three main selections were selected. The selection is a set of faces or cells where boundary conditions and initial conditions are defined. Then the volume is meshed in the Fire FAME HEXATM which is a component of AVL FIRETM software. The maximum cell size is 0,18 mm. Moreover, the area of the inlet and the outlet selections have two times smaller cell size. The model has 502.804 cells. The mesh is then imported back to Workflow Manager. The figure 4.1 shows the meshed volume with selections. The run mode of the solver is a crank angle

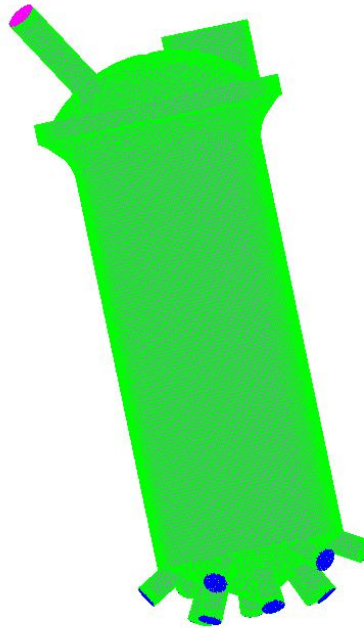


Figure 4.1: Grid with selections

based. The start at 0° is at the TDC at the end of the compression stroke, hence the highest pressure occurs here. In reality the first cycle has not a meaningful value in a point of view of the combustion. On the other side, in this case the combustion module is off thus the first cycle already shows important information to the task. The calculation deals with following assumptions:

- Engine speed: 1.800 RPM
- Combustion module is off
- Crankshaft angle step: $0,5^\circ$ which corresponds to $0,46 \cdot 10^{-4}$ s
- The mixture of air and methane is an ideal compressible gas
- k- ϵ turbulence model is used
- Species transport module is activated
- Potential flow initialization mode is activated
- The fuel is methane
- Boundary conditions are crank angle based

Boundary conditions such as the temperature, the pressure and the mass flow of methane have to be non-negative values. The ball check valve is replaced by the boundary condition "REF_inlet" where the flow profile shown in the figure 4.2

(black dashed line) is obtained from the GT-Power simulation validated by the mentioned experiment. The temperature is fixed at 330 K. The fuel mass fraction is set as 1 which means that only methane flows through the inlet boundary. The second boundary condition is "REF_outlet" which represents the area of twelve orifices connecting the chamber with the cylinder. This boundary condition is defined by the static pressure shown in the figure 4.2 (blue line) and the temperature in the cylinder shown in the figure 4.2. The temperature profile at the outlet selection is from GT-Power model too. The EGR mass fraction is set as 0 because the simulation doesn't contain the combustion. The gas inflow, the static pressure and the temperature profiles are same for all cycles and that is why only one cycle is shown.

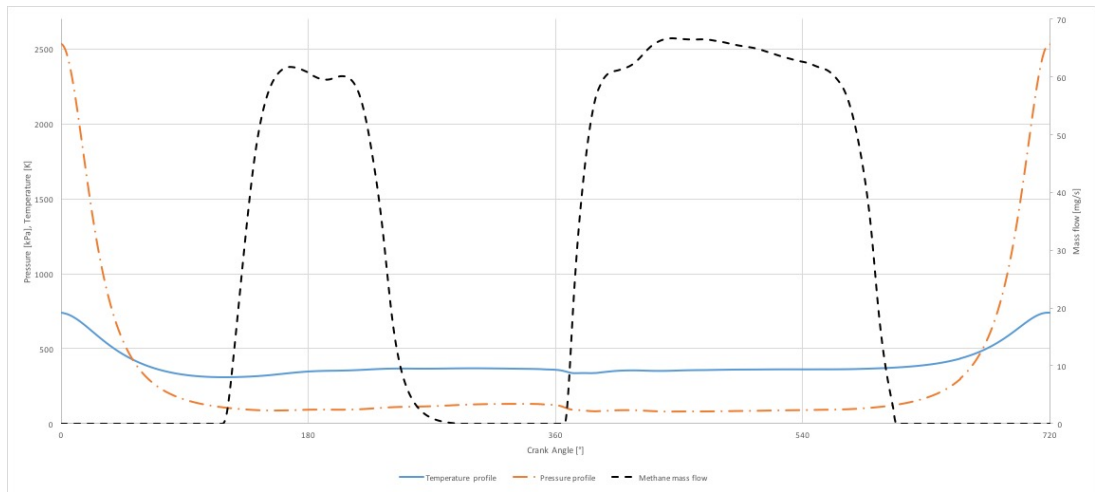


Figure 4.2: Boundary conditions - pressure, temperature and methane mass flow

The under relaxation factors are set with respect to the base setting of the software and the literature [4]. The under relaxation factor for the momentum is 0,2 in the range of the crankshaft angle of 0° and 5° , then 0,4 in the range of the crankshaft angle of 5° and 10° and for the rest of the simulation it is 0,65. Similarly for the pressure it is 0,2 up to 5° of a crankshaft and then 0,3 until the end. Turbulent kinetic energy and turbulent dissipation rate have an under relaxation factor of 0,5 for whole the simulation. The energy and species transport equations have an under relaxation factor of 0,8 for the whole simulation. The mass source, the viscosity and the scalar equations have an under relaxation factor of 1 for the whole simulation. The convergence criteria are set for the pressure and for the momentum. The value for the pressure is 0,004 and for the momentum 0,015. Maximum number of iteration per each step is 500. The figure 4.1 shows the meshed volume with selections.

4.2 Results

The highest impact on the result is given by the accuracy of chosen boundary conditions and initial conditions. The accuracy of the result is also given by convergence criteria, under relaxation factors and the quality of the grid. These all criteria are closely connected with a computational time. It is necessary to find an optimal settings to get results accurate enough with respect to a sufficiently short time period. The scavenging is important mainly in the surrounding of the spark plug where a fresh gas pushes out residual gases from a previous cycle. The quality scavenging and methane leakages are possible to investigate by the mass fraction of methane. The correct scavenging increases an efficiency of the combustion. In the beginning of the simulation the volume of the chamber is fulfil only by air. The gas is injected during the expansion and mainly during the intake stroke and that is why only methane, nitrogen and oxygen is shown. The mass fraction of the other elements is very close to zero. The specialist of the thesis created a similar CFD model using Ansys Fluent [20].

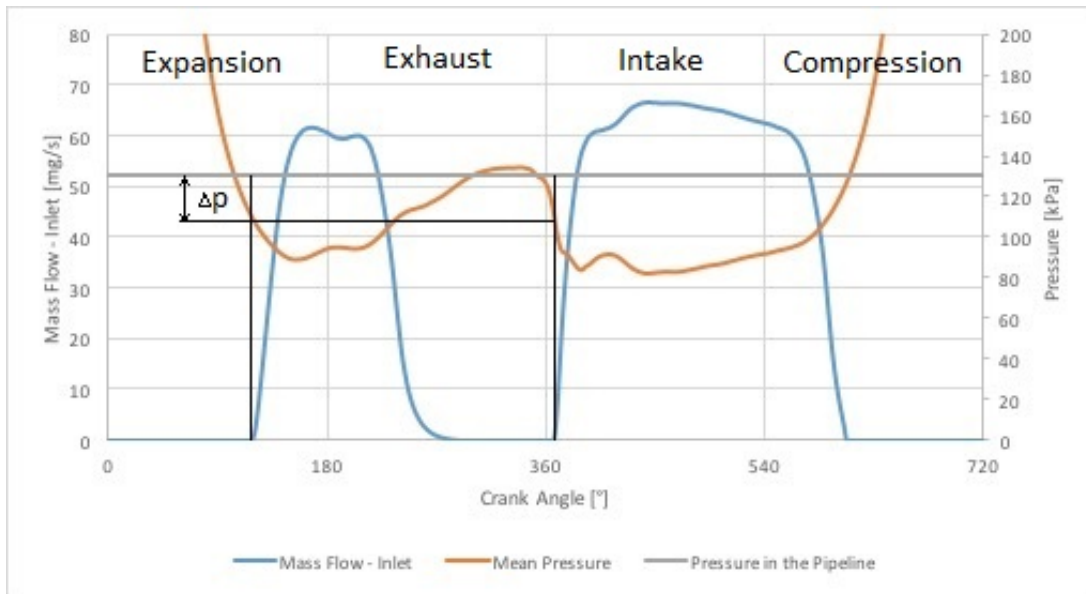


Figure 4.3: Cracking pressure of the valve

In the figure 4.3 is shown an inflow of methane during the expansion stroke. It indicates useless and unwanted leakages of methane during the exhaust stroke while the exhaust valve is opened. It is important to understand the cracking pressure of the ball check valve. The cracking pressure is the value of the pressure difference when the ball is pushed out and the gas flows freely through the valve to the chamber. In the figure 4.3 is visible that the gas flows when the pressure inside the chamber is lower than the pressure inside the gas pipeline. The value of the difference Δp is 20 kPa in this case. The pressure inside the pipeline is approximately 130 kPa thus the pressure inside the chamber has to fall below 110 kPa to unblock the way [20]. The data says that this pressure occurs approximately at 117° during the expansion stroke. It is explained at the figure 4.3. The inlet selection is in the top of

the chamber. The gas flows from the pipeline through the ball check valve into the chamber. In the figure 4.4 is the investigation of methane leakage. The orange line is an integral amount of the methane injected to the pre-chamber and the blue line shows the methane which left the pre-chamber during the cycle. The result is that

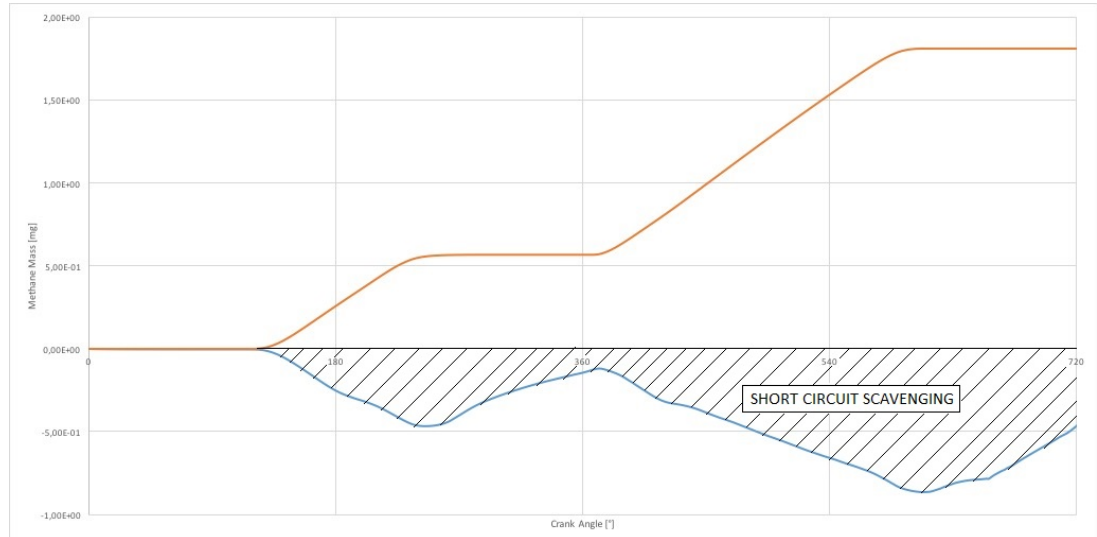


Figure 4.4: Methane integral mass inflow and the leakage

43,4 % of injected methane leaves the pre-chamber into the cylinder. The simulation using Ansys Fluent shows the leakage of 37 % [20]. Unfortunately, it is not possible to say if gas stays in the cylinder or leaves into the exhaust manifold. The figure 4.5 shows the mass fraction of the methane inside the pre-chamber in four different positions of the crankshaft during the expansion stroke.

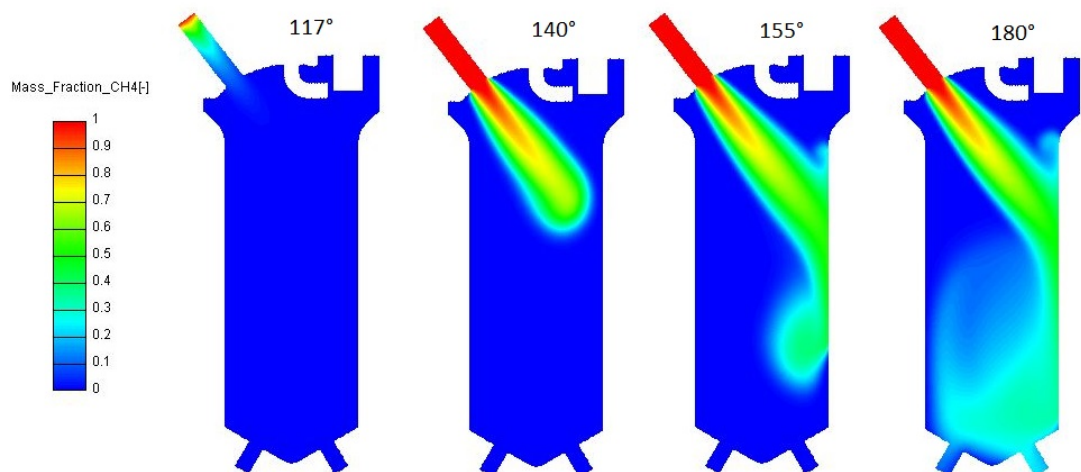


Figure 4.5: The injection during the expansion stroke

It shows the start of the injection and its ongoing propagation until it reaches the BDC where the piston changes a direction of the movement and the gas is pushed back to the chamber during the exhaust stroke. The figure 4.6 shows how the mixture flows through the outlet selection. It shows that only a very little volume of the mixture

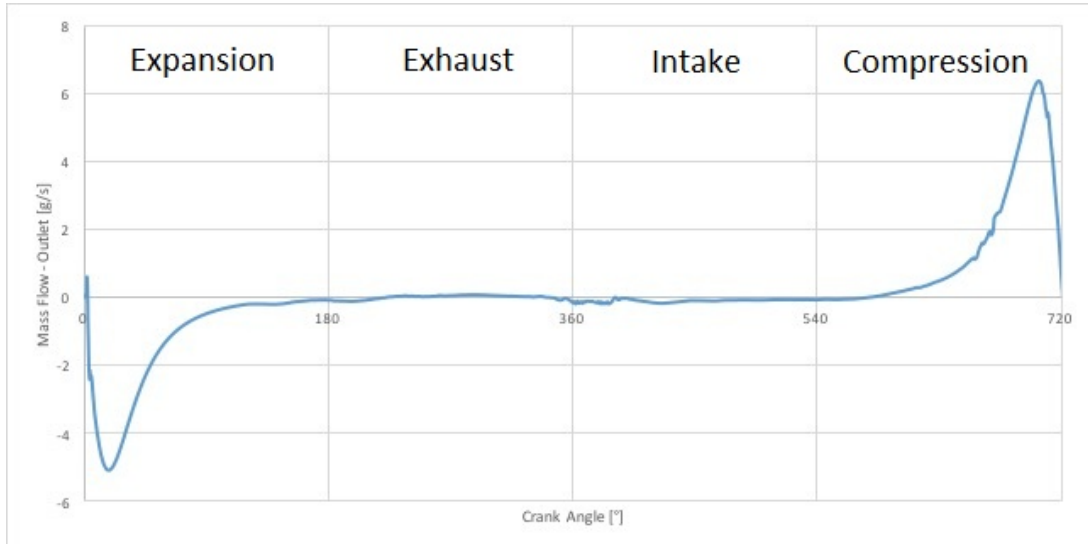


Figure 4.6: Mass flow of the mixture through the outlet selection

flows through the outlet selection. At the BDC after the expansion stroke is the mass fraction of methane 12,5 %. The second injection starts 6° after the start of the intake stroke. At this phase a significantly higher quantity of methane flows into the chamber. The dilution between methane, nitrogen and oxygen is visible in the figure 4.8.

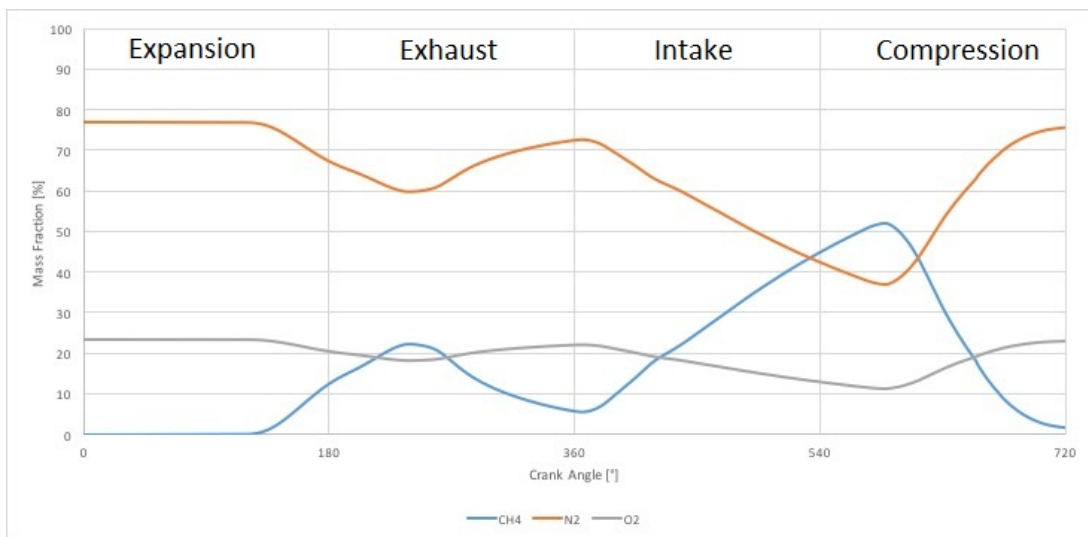


Figure 4.7: Mass fraction of main components

Methane starts to flow through all outlet orifices into the main combustion chamber 70° after the TDC of the exhaust stroke. The highest amount of methane occurs 228° after the TDC of the exhaust stroke where the chamber contains almost 52 % of the mass fraction of methane. The mass fraction of methane, oxygen and nitrogen which are represented in this simulation are shown in the figure 4.7.

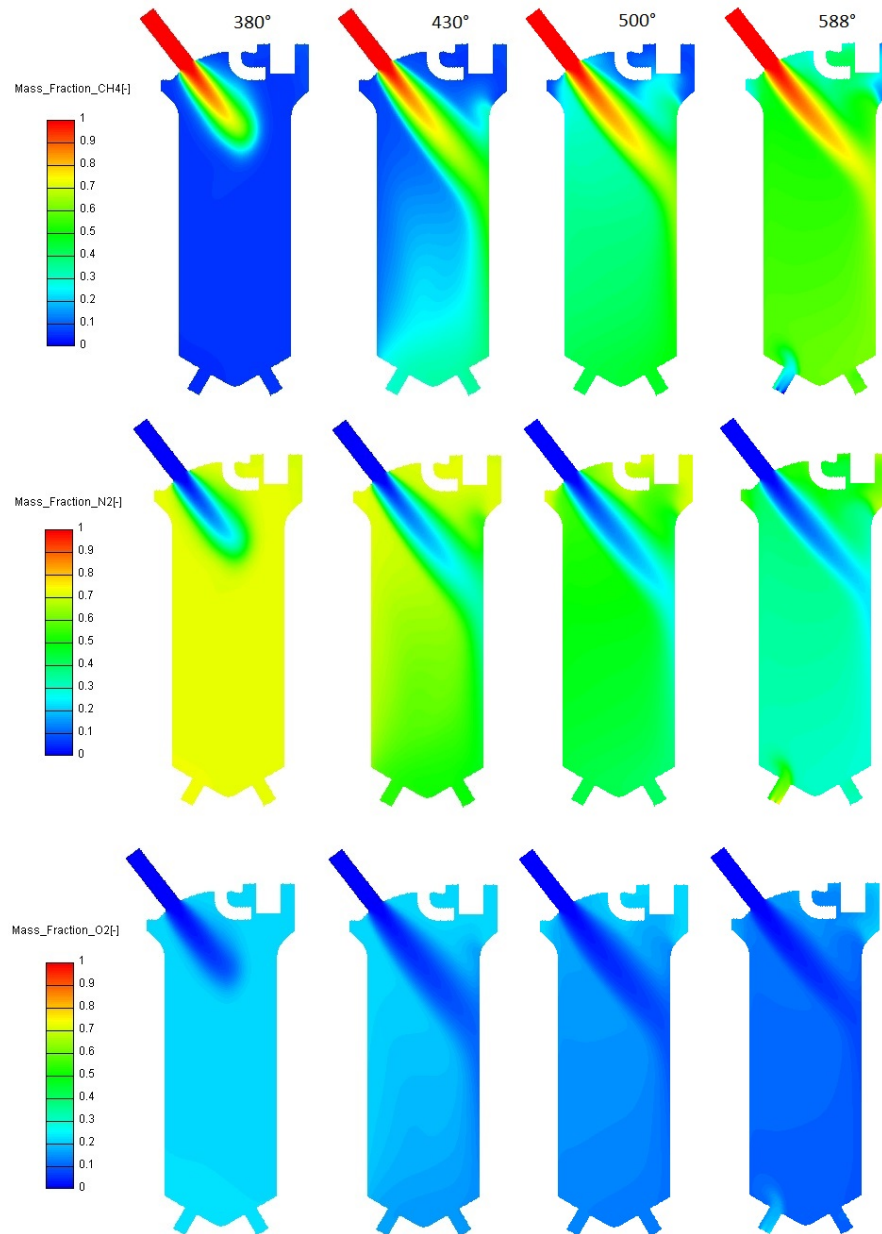


Figure 4.8: The Main injection during the intake stroke

Chapter 5

Conclusion

I acquainted with main features of natural gas, its extraction, advantages as well as disadvantages for the mobility. The pre-chamber indirect injection system and the concept of the lean combustion are a suitable way how to decrease harmful emissions of nitrogen oxides due to lower temperature of the combustion. The lower temperature is achieved due to a possibility of burning a very lean mixture and mixing with EGR gasses. Another advantage is that natural gas contains more energy than gasoline in the same volume. All these factors cause that the fuel consumption would considerably decrease.

The thesis itself has two parts. The main aim of the thesis was to create a 3-D CAD model of the pre-chamber ignition system and the drawing documentation using the software PTC Creo. The second aim was to prepare and test 3-D CFD model using the software AVL FireTM.

The design part describes completely new generation of the pre-chamber ignition system. The main changes compared to the original design are:

- Centrally mounted spark plug
- Spark plug without any modification
- Symmetrically distribution of gas
- The volume of the chamber increased to 6,2 % of the overall combustion volume
- Modularity of the design
- Two design versions
- Designed for all four cylinders

The centrally mounted spark plug without modifications solves the problem of the ignition stated in the preface. A very important improvement in the design is the channel which allows the symmetrical distribution of the gas and better scavenging in the surrounding of the spark plug. The volume of the chamber is more than two times higher than the original design. Two versions are designed. The version with the pressure transducer is for one cylinder only. For the rest three cylinders is the version without the transducer. It makes the design cheaper and easier to produce. Both versions are designed so that the module could be mounted or removed as one part. The design of the chamber made in 3-D CAD software is used for creating of the 3-D CFD model, hence it is possible to easily create many variants of design

and compare them quickly. The main advantage of the 3-D CFD simulation is that it is possible to compare many different variants without producing and testing expensive prototypes. Moreover, it is possible to study what is happening inside the chamber during the whole cycle. The model is prepared, meshed and tested. The simulation runs without the combustion. The further analysis and the comparison is out of the scope of the thesis. The simulation focuses on the methane leakages and the scavenging of the pre-chamber. The boundary conditions and initial conditions are based on the 1-D GT-Power model calibrated by experimental data. It is the reason why the CFD model is based on the older design. The main results of 3-D CFD part are as follow:

- The leakage of methane into the cylinder is 43,4 %
- Methane flows into the chamber during an expansion and an intake strokes
- The maximum mass fraction of methane inside the chamber is 51,8 %

It is shown that the cracking pressure of the ball check valve enables to flow the gas to the chamber during the expansion stroke. The leaked mass fraction of methane is 43,4 % which is slightly more than the leakage of 37 % in the similar model [20]. The maximum mass fraction of methane is almost 52 % and it occurs at 228° after the start of an intake stroke.

For further research is desirable to optimize the amount of cells to achieve an optimal compromise between the accuracy of results and the computational time. It takes more time in the beginning but later on it saves a lot of computational time. The stability of the calculation is influenced by initial conditions, time step and also by the quality of the grid. It is useful to compare results with a very similar model using different software. The most important step forward is to include the combustion. The mixture is completely different before an ignition as well as after the combustion. It is good to know if the mixture is stratified or homogeneous before the ignition. Moreover, the mixture is diluted by EGR gasses. The simulation of the combustion is very difficult in point of view of the chemical kinetics. A carbon monoxide, a carbon dioxide and unburned hydrocarbons are new gases in the mixture next to methane, oxygen, nitrogen monoxide and nitrogen dioxide. There are several possible or already proposed changes in the design which are desirable to simulate and compare them with a current solution and how they affect the formation of the mixture and the quality of the combustion:

- New design described in the thesis
- Simulation including the combustion
- The quality of scavenging due to two injection points
- The higher volume of the chamber
- The position of a spark plug
- Various volume of EGR gasses
- The gas flowing from the intake manifold
- Bi-fuel configuration of the engine

References

- [1] AKROS s.r.o. *Stainless Steel Tubes*.
Available at: <<http://www.akros.cz/trubky-kruhove-bezesve-mat-1-4435>>
- [2] ATTARD, William. *Turbulent Jet Ignition Pre-chamber Combustion System for Spark Ignition Engines* [online]. Inventor: William Attard. 01. 11. 2011. US 20120103302 A1.
Available at: <<http://www.google.com/patents/US20120103302>>
- [3] DAEWOO-AVIA *Engine D432: Service Manual*.
- [4] FERZIGER, J.H and Milovan PERIC. *Computational Methods for Fluid Dynamics*. Springer, third, rev edition, Berlin; Heidelberg; New York; Barcelona; Hong Kong; London; Milan; Paris; Tokyo, 2002. ISBN 3-540-42074-6
- [5] GE Jenbacher & Co Og. *Prechamber System* [online]. Inventor: Christoph Redtembacher. 19. 02. 2013. US 20130160734 A1
Available at: <<http://www.google.com/patents/US20130160734>>
- [6] HEYWOOD, John. B. *Internal Combustion Engine Fundamentals*. McGraw-Hill series in mechanical engineering, printed in USA. McGraw-Hill, New York, 1988. ISBN 0-07-028637-X
- [7] HIRSCH, Charles. *Numerical Computation of Internal & External Flows: Volume 1 The Fundamentals of Computational Fluid Dynamics*. Butterworth-Heinesmann, printed in Great Britain ,second edition, 2007. ISBN 978-0-7506-6594-0
- [8] KADLEČEK, Martin. *DP 2015 - SM 01: Analýza teplotního a mechanického namáhání plynového motoru s nepřímým zážehem*. Praha, 2015. Diplomová práce. ČVUT v Praze. Vedoucí práce Ing. Jiří Vávra, PhD.
- [9] LEE CO. *558 Series Check Valve Forward Flow*. Available at:
<<http://www.leeimh.com/metal/check-valves-axial/check-valve-558F.htm>>
- [10] LEINVEBER, Jan and Pavel VÁVRA. *Strojnické tabulky: Pomocná učebnice pro školy technického zaměření*. Úvaly, 2005. ISBN 80-7361-011-6.
- [11] MRŇA, Libor. *Technologie využívající laser* [online]. Brno, 2013.
Available at: <<http://ust.fme.vutbr.cz/svarovani/opory>>

- [12] MWM GmbH. *Spark Plug* [online]. Inventor: Olaf Berger. 25. 07. 2012. EP 2 690 726 A1.
Available at: <<http://www.freepatentsonline.com/EP2690726.pdf>>
- [13] NATGAS. Natural Gas: Overview of Natural Gas *Natural Gas.org* [online]. 20. 9. 2013.
Available at: <<http://naturalgas.org/overview/background/>>
- [14] NATGAS. Natural Gas: From Wellhead to Burner Tip *NaturalGas.org* [online]. 20. 09. 2013.
Available at: <<http://naturalgas.org/naturalgas/extraction-offshore/>>
- [15] PASHIN, Yu. V. and L. M. BAKHITOVA. Mutagenic and Carcinogenic Properties of Polycyclic Aromatic Hydrocarbons. *Environmental Health Perspectives* [online]. 1979(30), 185-189. Available at: <ncbi.nlm.nih.gov/pmc/articles/PMC1637690/pdf/envhper00475-0175.pdf>
- [16] RUBENA NÁCHOD a.s. *O-rings*.
Available at: <<http://eshop.rubena.cz/o-krouzky/c-2214/>>
- [17] Reciprocating Engines: Emission Control *PetroWiki.org* [online].
Available at: <<http://petrowiki.org/Reciprocating-engines>>
- [18] RWE Česká republika a.s. Zemní plyn a jeho druhy *RWE Česká republika a.s.* [online].
Available at: <<https://www.rwe.cz/o-rwe/zemni-plyn/>>
- [19] SOUČEK, Libor. *D 93 - M 15: Nepřímý zážeh pro průmyslový plynový motor*. Praha, 1993. Diplomová práce. ČVUT v Praze. Vedoucí práce Doc. Ing. Jan Macek, DrSc.
- [20] SYROVÁTKA ZBYNĚK, M. TAKÁTS and J. VÁVRA. *CFD Simulation of Scavenged Pre-chamber* [Submitted to KOKA 2016].
- [21] ŠŤOURAL, Martin. *DP 2014 - SM06: Zapalovací komůrka pro plynový motor s nepřímým zážehem*. Praha 2014. Diplomová práce. ČVUT v Praze. Vedoucí práce Ing. Jiří Vávra, PhD.
- [22] TRYGGVASON, Grétar. *The Equations Governing Fluid Motion* [online]. Notre Dame, 2013.
Available at: <www3.nd.edu/~gtryggva/CFD-Course/2013-Lecture-4.pdf>
- [23] VÁVRA Jiří, M. TAKÁTS, V. KLÍR and M. ŠKAROHLÍD. *Influence of Natural Gas Composition on Turbocharged Stoichiometric SI Engine Performance*. SAE Technical Paper 2012-01-1647, 2012.
- [24] WILCOX, David C. *Turbulence Modeling for CFD*. DCW Industries, Inc., California, 1993. ISBN 0-9636051-0-0

List of Figures

1.1	Position of the spark plug [21]	11
2.1	Pre-chamber scheme	14
2.2	Amount of emission versus air/fuel ratio [17]	15
2.3	Offshore drilling platforms [14]	17
2.4	Detailed cross-section of TJI system [2]	19
2.5	Partial cross-section of TJI system [2]	20
2.6	NO _x comparison of TJI and conventional SI engine [2]	21
2.7	CO comparison of TJI and conventional SI engine [2]	21
2.8	HC comparison of TJI and conventional SI engine [2]	22
2.9	MWM GmbH spark plug [12]	22
2.10	MWM GmbH pre-chamber system [12]	23
2.11	Detail of the CKD design [19]	24
2.12	GE Jenbacher GmbH [5]	25
2.13	Engine Daewoo-Avia [3]	26
2.14	Tedom stationary gas engine [21]	27
2.15	The cross-section of the cylinder Head [21]	28
2.16	Module of a Pre-chamber [21]	29
2.17	The ceramic insulator and the central electrode [21]	30
3.1	Cylinder head of an engine D432 series	32
3.2	Cross-section of an improved cylinder head with o-rings	32
3.3	Chamber	33
3.4	Volume of the chamber	34
3.5	Module housing	36
3.6	Weldment preform - bottom part	37

3.7	Weldment preform - top part	37
3.8	Spark plug socket	38
3.9	Insertion	38
3.10	Gas elbow	39
3.11	Upper housing	40
3.12	Bronze wool	41
3.13	Spark plug NGK ER8EXIX M8x1	41
3.14	Oprand M3x0.5 pressure transducer	42
3.15	Ball check valve LEE 558 series	43
3.16	Step by step assembly	44
3.17	Complete module	45
3.18	Gas supply sub-assembly	46
3.19	Complete assembly	47
3.20	Spark plug socket without a pressure transducer	48
3.21	Insertion without a pressure transducer	49
3.22	Gas Elbow without a pressure transducer	49
3.23	Upper housing without a pressure transducer	50
3.24	Complete Assembly without a pressure transducer	51
4.1	Grid with selections	57
4.2	Boundary conditions - pressure, temperature and methane mass flow	58
4.3	Cracking pressure of the valve	59
4.4	Methane integral mass inflow and the leakage	60
4.5	The injection during the expansion stroke	60
4.6	Mass flow of the mixture through the outlet selection	61
4.7	Mass fraction of main components	61
4.8	The Main injection during the intake stroke	62

List of Tables

2.1	Composition of natural gas [18]	18
2.2	Daewoo-Avia D432 parameters [3]	26

List of Attachments (Inside the Thesis):

Attachment 1: 1.4878 Material Sheet

Attachment 2: 1.0070 Material Sheet

Attachment 3: 2.0060 Material Sheet

Attachment 4: 1.0036 Material Sheet

Attachment 5: 1.4541 Material Sheet

Attachment 6: 1.1191 Material Sheet

Attachment 7: 1.4435 Material Sheet

Attachment 8: PTFE Material Sheet

Attachment 9: Pressure Transducer Optrand

Attachment 10: Ball Check Valve Lee 558 Series

Attachment 11: Rubena NÄ~chod a.s. Catalogue Lists

List of Attachment (Outside the Thesis):

Name	Drawing Number
CYLINDER_HEAD_ASSEMBLY	3-001_ASM
CYLINDER_HEAD_ASSEMBLY_WO	3-001-W/O-ASM
MODULE_SUB-ASSEMBLY	3-002-SUBASM
MODULE_SUB-ASSEMBLY_WO	3-002-W/O-SUBASM
GAS_SUPPLY_SUB-ASSEMBLY	4-003-SUBASM
WELDMENT_SUB-ASSEMBLY	3-004-SUBASM
CLAMP_SUB-ASSEMBLY	4-005-SUBASM
MODULE_HOUSING	4-006-SUBASM
CYLINDER_HEAD-MODIFIED	3-000
CHAMBER	3-001
COVERING_TUBE	4-002
SPARK_PLUG_SOCKET	3-003
SPARK_PLUG_SOCKET_WO	3-003-W/O
INSERTION	4-004
INSERTION_WO	4-004-W/O
GAS_TUBE	4-005
PAD	4-006
GAS_ELBOW	3-007
GAS_ELBOW_WO	3-007-W/O
UPPER_HOUSING	3-008
UPPER_HOUSING_WO	3-008-W/O
SPARK_PLUG_TERMINATION	4-009
TEFLON_BUSHING	4-010
GAS_TUBE_2	4-011
GAS_TUBE_TERMINATION	4-012
CLAMP	3-013
COVER	4-014
BUSHING	4-015
WELDMENT_PREFORM_TOP	4-016
WELDMENT_PREFORM_BOTTOM	3-017
3-D CFD Model	

Attachment 1: 1.4878 Material Sheet



ThyssenKrupp Materials International

Austenitic Heat Resisting Steel

Material Data Sheet

Steel designation:	Name	Material No.
	X8CrNiTi18-10	1.4878

Scope

This data sheet applies for hot and cold rolled sheet and strip and bars, semi-finished products, rods and sections.

Application

For construction parts which should be resistant to scaling up to about 850 °C and extensively inured to the effect of sulfurous gases. Inclination to carburization in reduced gases is very low.

Chemical composition (Heat analysis in %)

Product form	C	Si	Mn	P	S	Cr	Ni	Ti
C, H, P, L	≤ 0,10	≤ 1,00	≤ 2,00	≤ 0,045	≤ 0,015	17,00-19,00	9,00-12,00	5x%C ≤ 0,80

C = cold rolled strip; H = hot rolled sheet; P = hot rolled sheet; L = semi-finished products, bars, sections

Mechanical properties at room temperature in the solution annealed condition

Product form	Thickness <i>a</i> or Diameter <i>d</i> mm	HB max. (1/2)3	Proof strength ¹⁾		Tensile strength <i>R_m</i> N/mm ²	Elongation A % min.		
			<i>R_{0,2}</i> N/mm ²	<i>R_{0,01}</i> N/mm ²		Long products ²⁾	Flat products	
							0,5 ≤ <i>a/d</i> < 3	3 ≤ <i>a/d</i>
C, H, P	<i>a</i> ≤ 12	215	190	230	500 - 720	40 ³⁾	40 ⁴⁾⁵⁾	40 ⁴⁾⁶⁾
L	<i>d</i> ≤ 25							

¹⁾ The maximum HB values may be raised by 100 units or the maximum tensile strength value may be raised by 200 N/mm² and the minimum elongation value be lowered to 20 % for cold worked sections and bars of ≤ 35 mm thickness.

²⁾ For guidance only.

³⁾ For rod, only the tensile values apply.

⁴⁾ Longitudinal test piece ⁵⁾ Transverse test piece

⁶⁾ After cold forming the elongation for wall thicknesses ≤ 35 mm amounts to minimum 20 %.

⁷⁾ Bars ⁸⁾ Rods and sections

Creep properties - estimated average values about the long-term behavior at elevated temperature*

Temperature °C	1 %-Elongation ¹⁾ for		Rupture ²⁾ for		
	1000 h	10 000 h	1000 h	10 000 h	100 000 h
	N/mm ²		N/mm ²		
600	110	85	200	142	65
700	45	30	88	48	22
800	15	10	30	15	10

¹⁾ Stress related to the out put cross-section, which leads after 1000 or 10 000 h to a permanent elongation of 1 %.

²⁾ Stress related to the out put cross-section, which leads after 1000, 10 000 or 100 000 h to breakage.

* for guidance only

Attachment 2: 1.0070 Material Sheet

Quality	E360 (Fe 690 - C50E - C55E - C60E)						
According to standards	EN 10025-2: 2004						
Number	1.0070						
Chemical composition							
C%	Si%	Mn%	P% max	S% max	N% max	Cu%	
			0,045	0,045	0,012 ^{a)}	Cast analysis	
			0,055	0,055	0,014 ^{b)}	Product analysis	
FN deoxidation method - rimming steel not admitted							
^{a)} N max value is not applied if chemical composition shows total Al content of 0.020%							
^{b)} N max value is not applied if chemical composition shows total Al content of 0.015%							
Temperature °C							
Hot-forming	Normalizing +N	Quenching +Q	Quenching +Q	Tempering +T	Temperature values are valid for analysis close to:		
1050-850	825-885 air	830 water	850 oil, polymer	550-650 air	C% ~ 0.52	Mn% ~ 0.80 Si% ~ 0.30	
				Pre-heating welding	Stress-relieving after welding		
Soft annealing +A	Isothermal annealing +I	Stress- relieving +SR	End quench hardenability	250	600 furnace cooling		
690 air	790 furnace cooling to 660 then air	50 under the temperature of tempering		Ac1	Ac3	Ms Mf	
Mechanical properties							
Hot-rolled EN 10025-2: 2004 E360 1.0070							
Testing at room temperature							
size mm	R	ReH	A% L	A% T	Kv	HB	
from to	N/mm ²	N/mm ² min	min	min	J min	for information	
3	690-900	360					
16	670-830	360	11	10		203-249	
40	670-830	355	11	10		203-249	
63	670-830	345	10	9		203-249	
80	670-830	335	9	8		203-249	
100	670-830	325	9	8		203-249	
150	650-830	305	8	7		200-249	
200	640-830	295	7	6		198-249	
250	640-830	285	7	6		198-249	
+N normalization is suggested							
Cold-drawn +C					Hot rolled - Peeled Reeled +SH		
size mm	Testing at room temperature (longitudinal)				Testing at room temperature (longitudinal)		
	R ^{c)}	Rp 0.2 ^{c)}	A%	HB	R	Rp 0.2 A% HB	
from to	N/mm ²	N/mm ² min	min		N/mm ²	N/mm ² min min	
No indications from reference standards.							
EUROPE	ITALY	CHINA	GERMANY DIN	FRANCE AFNOR	U.K.	RUSSIA	USA
EN	UNI	GB			B.S.	GOST	AISI/SAE
E360	Fe 690		E360	A 70-2	E360		

THE DATA CONTAINED HEREIN ARE INTENDED AS REFERENCE ONLY AND ARE SUBJECT TO CONSTANT CHANGE. LUCEFIN S.P.A. DISCLAIMS ANY AND ALL LIABILITY FOR ANY CONSEQUENCES THAT MAY RESULT FROM THEIR USE.

Attachment 3: 2.0060 Material Sheet

1/1

Data sheets // E-COPPER // 7



Brand Name	E-COPPER			
Material Code	CW004A/2.0060			
Abbreviation	Cu-ETP (formerly: E-Cu57)			
Chemical Composition (mass components) in %.				
Average values of alloy components				
Cu				
≥ 99.9				



Features and Application Notes

E-COPPER is especially characterized by high conductivity and relatively high corrosion resistance. Like all pure metals, E-COPPER has a high temperature coefficient. The most important properties are listed only for reasons of completeness. Copper is normally supplied for thermocouples and compensation cables for protective switches. The maximum working temperature in air is +150 °C. When used as wire for thermoelectric applications, the maximum temperature can be up to +350 °C.

Form of Delivery

E-COPPER is supplied in the form of round wires in the range 0.10 to 3.00 mm Ø in bare condition. To a limited extent insulated wires, stranded wires and strips are also manufactured.

Electrical Resistance in Annealed Condition

Temperature coefficient of electrical resistance between +20 °C and +105 °C 10 ⁻⁴ /K	Electrical resistivity in: μΩ x cm (first line) and Ω/CMF (second line) Reference Values					
	+20 °C tolerance ±10 %	+100 °C	+200 °C	+300 °C	+400 °C	+500 °C
approx. + 4,300	1.72	2.30	3.10			
	10	14	19			

Physical Characteristics (Reference Values)

Density at +20 °C	Melting point	Specific heat at +20 °C	Thermal conductivity at +20 °C	Average linear thermal expansion coefficient between +20 °C and +100 °C		Thermal EMF against copper at +20 °C
g/cm ³	lb/cub in	°C	J/g K	W/m K	10 ⁻⁶ /K	10 ⁻⁶ /K
8.90	0.32	1,083	0.38	390.00	17.50	18.50
						0.00

Strength Properties at +20 °C in Annealed Condition

Tensile Strength ²⁾		Elongation (L _g = 100 mm) % at nominal diameter in mm				
MPa	psi	0.020 to 0.063	> 0.063 to 0.125	> 0.125 to 0.50	> 0.50 to 1.00	> 1.00
200	29,000	= 10	= 15	= 20	≥ 25	≥ 30

General Note // E-COPPER is not a standard resistance alloy. Therefore no resistance values are quoted. The weight values correspond to those of ISOTAN® wires of the same diameter.

1) The resistivity at 0 °C is 1.56 μΩ x cm.

2) This value applies to wires of 2.0 mm diameter. For thinner wires the minimum values will substantially increase, depending on the dimensions.

Attachment 4: 1.0036 Material Sheet

ČSN 11373 – plain carbon structural steel



1. Guideboard of other standards

DIN	EN 10027-1	EN 10027-2	EN 10025:90	GOST
UST37-2	S235JRG1	1.0036	Fe360BFU	St2kp

2. Chemical composition (heat analysis) in %

C	Mn	Si	P	S	N	Al
max. 0,170			max. 0,045	max. 0,045	max. 0,007	

3. Mechanical properties

Mechanical properties	Execution	
	heat untreated	normalized
Tensile strength R_m [MPa]	min. 370	min. 350
Yield point R_e [MPa]	min. 250	min. 220
Ductility A_{10} [%]	min. 7	min. 20

4. Steel characterization and examples of usage

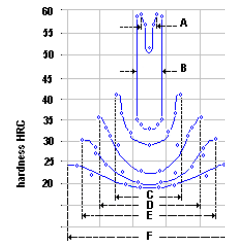
Plain carbon structural steel suitable for parts of constructions and machines with a medium thickness, fusion welded, statically stressed, possibly even lightly dynamically stressed. Forge welded parts. Suitable for less stressed welded pipes and branch pipes, weir constructions and dished, flat and high-pressure flanged bottoms.

Attachment 5: 1.4541 Material Sheet

Quality		X6CrNiTi18-10				Austenitic		
Number		1.4541				Stainless Steel		
<p style="text-align: right;">TECHNICAL CARD GRUPPO LUCEFIN REVISION 2012 ALL RIGHTS RESERVED</p>								
Chemical composition								
C% max	Si% max	Mn% max	P% max	S% ^{a)} max	Cr%	Ni%	Ti% max	
0,08	1,00	2,00	0,045	0,015	17,0-19,0	9,0-12,0	> 5 x C < 0,70	EN 10088-1: 2005
± 0.01	+ 0.05	± 0.04	+ 0.005	+ 0.003	± 0.2	± 0.1	± 0.05	
Product deviations are allowed								
^{a)} for improving machinability, it is suggested a controlled sulphur content of 0,015 % - 0,030 %								
Temperature °C								
Melting range	Hot-forming	Solution annealing (Solubilization) +AT	Stabilizing	Soft annealing +A	MMA welding – AWS electrodes pre-heating not necessary post welding slow cooling			
1430-1400	1200-1150	1120-1020 water	900-840 calm air	not suitable				
Sensitization	Quenching +Q	Tempering +T				joint with steel carbon CrMo alloyed stainless		
not suitable	not suitable	not suitable				E309-E308 E309-E308 E308-E347 cosmetic welding E347		
Mechanical properties								
Hot-formed EN 10088-3: 2005 in conditions 1C, 1E, 1D, 1X, 1G, 2D								
size Testing at room temperature								
mm	R	Rp 0.2	A% (L)	A% (T)	Kv +20 °C (L)	Kv +20 °C (T)	HB ^{a)}	
from to	N/mm ²	N/mm ² min	min	min	J min	J min	max	
160	500-700	190	40		100		215	+AT solubilization
160	250	500-700	190	30	60	215		+AT solubilization
^{a)} for information only (L) = longitudinal (T) = transversal								
Cold-processed EN 10088-3: 2005 in conditions 2H, 2B, 2G, 2P								
size Testing at room temperature								
mm	R	Rp 0.2	A% (L)	A% (T)	Kv +20 °C (L)	Kv +20 °C (T)		
from to	N/mm ²	N/mm ² min	min	min	J min	J min		
10	16	580-950	380	25				+AT solubilization
16	40	500-850	190	30	100			
40	63	500-850	190	30	100			
63	160	500-700	190	40	100			
^{b)} in the range of 1 mm ≤ d < 5 mm, values are valid only for rounds – the mechanical properties of non round bars of < 5 mm of thickness have to be agreed at the time of request and order (L) = longitudinal (T) = transversal								
Forged +AT solubilization								
size Testing at room temperature								
mm	R	Rp 0.2	A% (L)	A% (T)	Kv +20 °C	Kv +20 °C	Kv -196 °C	
from to	N/mm ²	N/mm ² min	min (L)	min (T)	J min (L)	J min (T)	J min (T)	
450	500-700	190	30	30	100	60		EN 10250-4: 2001
450	510-710	200	40	30	100	60	60	EN 10222-5: 2001
Work-hardened by cold-drawing EN 10088-3: 2005 in condition 2H (es. +AT+C)								
size Testing at room temperature								
mm	R	Rp 0.2	A%					
from to	N/mm ²	N/mm ² min	min					
35	700-850	350	20	+AT+C700 cold-drawn material				
25	800-1000	500	12	+AT+C800 cold-drawn material				
Transition curve determined by Kv impacts. Material solubilized at 1050 °C								
Average J	230	240	240	250	250	260	260	+AT material – Approximate values
Test at °C	-160	-120	-80	-40	0	+40	+80	°C R Rp 0.2 A
								N/mm ² N/mm ² %
								+24 500 200 401
								-80 855 300 35
								-196 1440 380 30
								-254 1645 630 20

Attachment 6: 1.1191 Material Sheet



Quality		C45E						Technical card	
According to standards		EN 10083-2: 2006						Lucefin Group	
Number		1.1191							
Chemical composition									
C%	Si% max	Mn%	P% max	S% max	Cr% max	Mo% max	Ni% max	Product deviations are allowed	
0,42-0,50 ± 0,02	0,40 + 0,03	0,50-0,80 ± 0,04	0,030 + 0,005	0,035 + 0,005	0,40	0,10	0,40		
Cr+Mo+Ni max 0.63%									
For C45R n° 1.1201, S% 0.020-0.040 product deviation ± 0.005									
For C45 n° 1.0503, P% - S% max 0.045									
On request, it may be supplied (Ca) treated									
Temperature °C									
Hot-forming	Normalizing	Quenching	Quenching	Tempering	Stress-relieving				
1100-850	870 air	840 water	860 oil or polymer	540-660 air	50° under the temperature of tempering				
Soft annealing	Isothermal annealing	Natural state	End quench hardenability test	Pre-heating welding	Stress-relieving after welding				
690 cooling 10 °C/h to 600, then air (HB max 207)	810 furnace cooling to 660, then air (HB 160-216)	(~ HB 169-245)	850 water	250	550 furnace cooling				
				AC1	AC3	Ms	Mf		
				735	780	350	120		
Mechanical and physical properties									
C45E C45R Hot-rolled mechanical properties in normalized condition EN 10083-2: 2006									
Testing at room temperature (longitudinal)									
size d / t mm	R	Re ^{a)}	A%	C%	Kv	HB			
from to	N/mm ² min	N/mm ² min.	min.	min.	J min.	min			
16/16	620	340	14			190			
16/16 100/100	580	305	16			172			
100/100 250/250	560	275	16			162			
d = diameter t = thickness									
C45E C45R Hot-rolled mechanical properties in quenched and tempered condition EN 10083-2: 2006									
Testing at room temperature (longitudinal)									
size d / t mm	R	Re ^{a)}	A%	C%	Kv	HB			
from to	N/mm ²	N/mm ² min	min.	min.	J min	for information			
16/8	700-850	490	14	35		213-253			
16/8 40/20	650-800	430	16	40	25	200-240			
40/20 100/60	630-780	370	17	45	25	192-232			
^{a)} Re upper yield strength or, if no yield phenomenon occurs, Rp 0.2 has to be considered									
d = diameter t = thickness									
Table of tempering values obtained at room temperature on rounds of Ø 10 mm after quenching at 850 °C in water					Hardness condition on bars quenched in water				
°C	HB	HRC	R N/mm ²						
100	615	58	2330	A = diameter 13 mm					
200	597	57	2240	B = diameter 25 mm					
300	510	52	1880	C = diameter 50 mm					
400	401	43	1390	D = diameter 75 mm					
500	311	33	1030	E = diameter 100 mm					
600	242	23	810	F = diameter 130 mm					
°C	R N/mm ²	Rp 0.2 N/mm ²	A %	• hardness check points					
620	740	480	22						
650	600	400	23						
700	540	320	24						



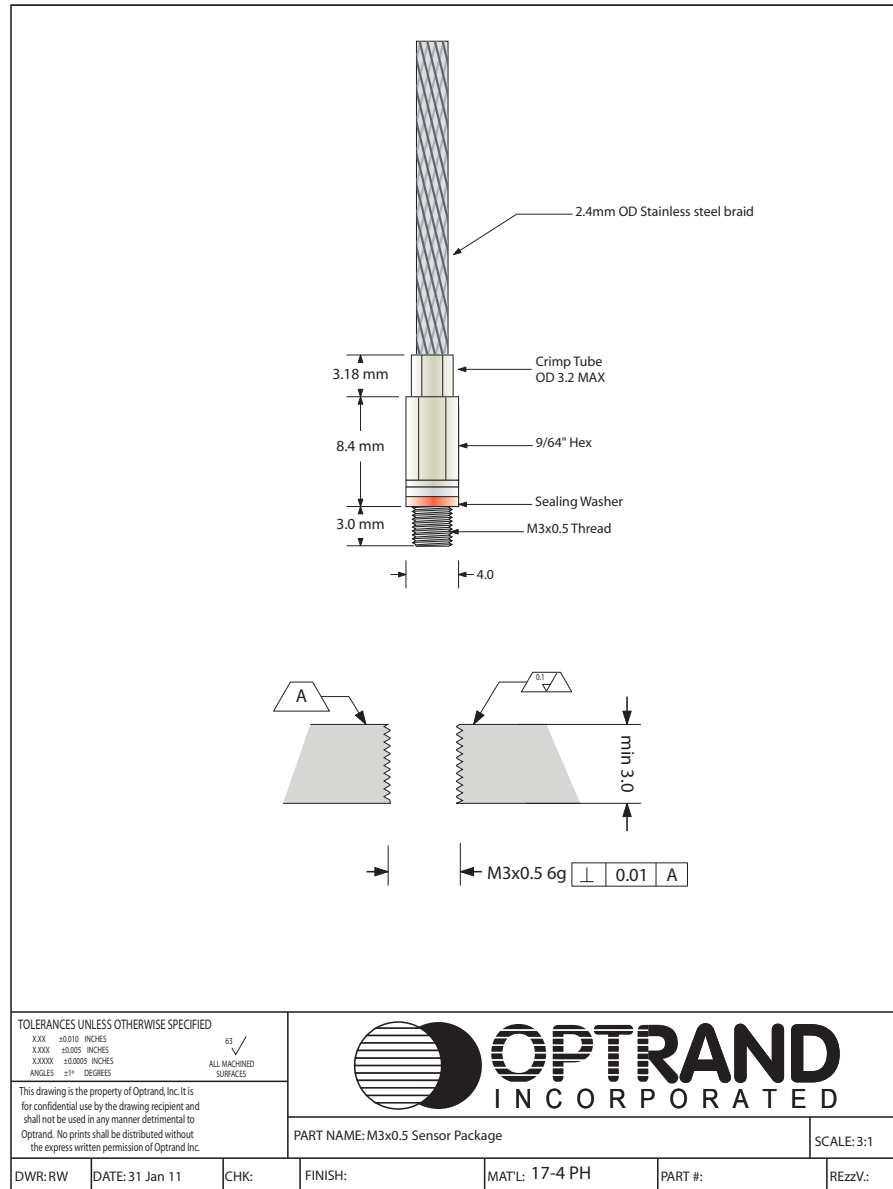
Attachment 7: 1.4435 Material Sheet

MATERIAL No.: 1.4435										
DESCRIPTION										
EN symbol (short)	X2CrNiMo18-14-3									
AISI	AISI 316L									
UNS	S 31603 Grade TP 316L									
AFNOR	NF EN 10297-12(12-2005)									
BS	B.S EN 10288-1 (06/2005)									
Registered work's label	Supra®									
Density lbs / cm ³	0,29									
Hardness HB30 Rockwell Hardness Number max.	<=215 B90 - 316L -(ASTM A249)									
Composition	chromium nickel molybdenum steels									
Category	Stainless steels steel, resistant to rust and acids									
Structure	austenitic									
Corrosion	resistant to intercrystalline corrosion good resistance to tensile corrosion non-corroding									
Description Increased corrosion resistance to halogenated substances and oxidising acids, due to it's high molybdenum content in comparison to 1.4401/1.4404.										
CHEMICAL COMPOSITION										
1.4435	C	Mn	P	S	Cr	Mo	Si	Ni	N	
	Min %				17,00	2,50		12,50		
	Max %	0,030	2,00	0,045	0,015	19,00	3,00	1,00	15,00	0,110
(Key to steel 2010)										
AISI 316L S 31603	Min %				16,0	2,0		10,0		
	Max %	0,035	2,0	0,045	0,030	18,0	3,0	1,0	15,0	
ASTM A 312 (TP 316L)										
PHYSICAL PROPERTIES										
Property	Value									
Density: lbs / cm ³	0,29									
Hardness: HB30 Rockwell Hardness Number max.	<=215 B90 - 316L -(ASTM A249)									
magnetizable	no									
resistant to intercrystalline corrosion	yes									
Temperature T °C / F (°C / F)	Specific heat J / kgK (Btu / lb °F)	Thermal conductivity W / mK (Btu-in / ft ² -h-°F)	Electric resistance μΩ · cm (Ω circ mill / ft)	Modulus of elasticity kN / mm ² (10 ³ ksi)	Expansion rate from 70°F bis T 10 ⁻⁶ / K (10 ⁻⁶ / °F)					
20 / 68	500	14,0 (8)	0,75	200 (29,0)						
100 / 212		14,6 (9)		194 (28,1)	16,0 (9,2)					
200 / 392		17,0 (10)		186 (27,9)	16,5 (9,5)					
300 / 572		18,0 (11)		179 (25,9)	17,0 (9,7)					
400 / 752		20,0 (13)		171 (24,8)	17,5 (10,0)					
500 / 932		21,0 (13)		164 (23,8)	19,0 (10,2)					
Temperature °C / °F	0,2% Yield strength in high temperatures Rp 0,2 MPa / ksi	1,0% Yield strength in high temperatures Rp 1,0 MPa / ksi	Tensile strength in high temperatures Rm							
100/212	165 / 23,9	200 / 29,0								
200/392	137 / 19,9	165 / 23,9								
300/572	119 / 19,2	145 / 21,0								

Attachment 8: PTFE Material Sheet

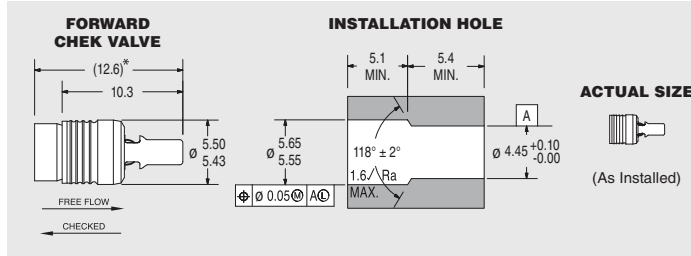
				
TEFLON				
<p>PolyTetraFluoroEthylene is a fluorocarbon-based polymer and is commonly abbreviated PTFE. The Teflon® brand of PTFE is manufactured only by DuPont. Several other manufacturers make their own brands of PTFE which can often be used as substitute materials. This fluoroplastic family offers high chemical resistance, low and high temperature capability, resistance to weathering, low friction, electrical and thermal insulation, and "slipperiness". (see also Teflon® PTFE and Teflon® FEP & PFA Specifications) PTFE's mechanical properties are low compared to other plastics, but its properties remain at a useful level over a wide temperature range of of -100°F to +400°F (-73°C to 204°C). Mechanical properties are often enhanced by adding fillers (see paragraph below). It has excellent thermal and electrical insulation properties and a low coefficient of friction. PTFE is very dense and cannot be melt processed -- it must be compressed and sintered to form useful shapes.</p>				
FILLED GRADES				
<p>PTFE's mechanical properties can be enhanced by adding fillers such as glass fibers, carbon, graphite, molybdenum disulphide, and bronze. Generally, filled PTFE's maintain their excellent chemical and high temperature characteristics, while fillers improve mechanical strength, stability, and wear resistance. The properties of 25% glass-filled and 25% carbon-filled PTFE grades are shown below for comparison purposes. There are literally dozens of different filled PTFE products and grades -- too many to be listed here. Please contact Boedeker Plastics for more information about other filled PTFE products for your application.</p>				
TYPICAL PROPERTIES of PTFE				
ASTM or UL test	Property	PTFE (unfilled)	PTFE (25% glass filled)	PTFE (25% carbon filled)
PHYSICAL				
	Density (lb/in ³)	0.078	0.081	0.075
D792	(g/cm ³)	2.16	2.25	2.08
D570	Water Absorption, 24 hrs (%)	< 0.01	0.02	0.05
MECHANICAL				
D638	Tensile Strength (psi)	3,900	2,100	1,900
D638	Tensile Modulus (psi)	80,000	-	-
D638	Tensile Elongation at Break (%)	300	270	75
D790	Flexural Strength (psi)	No break	1,950	2,300
D790	Flexural Modulus (psi)	72,000	190,000	160,000
D695	Compressive Strength (psi)	3,500	1,000	1,700
D695	Compressive Modulus (psi)	70,000	110,000	87,000
D785	Hardness, Shore D	D50	D60	D62
D256	IZOD Notched Impact (ft-lb/in)	3.5	-	-
THERMAL				
D696	Coefficient of Linear Thermal Expansion (x 10 ⁵ in./in./°F)	7.5	6.4	6
D648	Heat Deflection Temp (°F / °C) at 264 psi	132 / 55	150 / 65	150 / 65
D3418	Melting Temp (°F / °C)	635 / 335	635 / 335	635 / 335
-	Max Operating Temp (°F / °C)	500 / 260	500 / 260	500 / 260
C177	Thermal Conductivity (BTU-in/ft ² -hr-°F) (x 10 ⁴ cal/cm-sec-°C)	1.7	3.1	4.5
UL94	Flammability Rating	V-O	V-O	V-O
ELECTRICAL				
D149	Dielectric Strength (V/mil) short time, 1/8" thick	285	-	-
D150	Dielectric Constant at 1 MHz	2.1	2.4	-
D150	Dissipation Factor at 1 MHz	< 0.0002	0.05	-
D257	Volume Resistivity (ohm-cm)at 50% RH	> 10 ¹⁸	> 10 ¹⁸	104
<p>NOTE: The information contained herein are typical values intended for reference and comparison purposes only. They should NOT be used as a basis for design specifications or quality control. Contact us for manufacturers' complete material property datasheets.</p> <p>All values at 73°F (23°C) unless otherwise noted. TEFLON® is a registered trademark of DuPont</p>				

Attachment 9: Optrand M3x0,5 Pressure Sensor

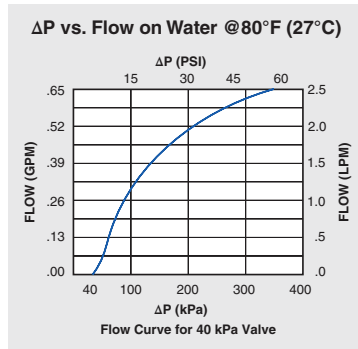


INSERT CHECK VALVES

558 SERIES CHEK VALVE - FORWARD FLOW



* LOA before installation.
All dimensions in millimeters.



PERFORMANCE	
Lohm Rate:	250 Lohms
Leakage:	20 sccm/min. (max.) @ 172 kPa (25 psid) on air
	1 Drop/min. (max.) on hydraulic fluid (MIL-PRF-83282)
Maximum Working Pressure:	28 MPa (4,060 psid) (Checked Direction)
	4 MPa (580 psid) (Flow Direction)

MATERIALS	
Body	303 Stainless Steel
Cage	305 Stainless Steel
Pin	416 Stainless Steel
Spring	302 Stainless Steel
Ball	440C Stainless Steel

LEE PART NO.	CRACKING PRESSURE
CCFM2550200S	0 kPa (No Spring)
CCFM2550204S	4 ± 3 kPa (0.6 ± 0.4 psid)
CCFM2550207S	7 ± 5 kPa (1 ± 0.7 psid)
CCFM2550214S	14 ± 5 kPa (2 ± 0.7 psid)
CCFM2550225S	25 ± 10 kPa (3.6 ± 1.5 psid)
CCFM2550240S	40 ± 30 kPa (6 ± 4.4 psid)
CCFM2550269S	69 ± 17 kPa (10 ± 2.5 psid)

INSTALLATION	
Tool Part Number	CCRT0900120S
Force	625 Kg F (max.)
View Installation Procedure	



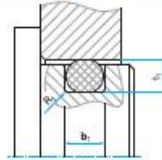
The Lee Company
Industrial Microhydraulics Group, 82 Pequot Park Road, Westbrook, CT 06498-0424
Tel: 860-399-6281 • www.leeimh.com • © 2009 by The Lee Company, USA

Attachment 11: Rubena a.s. Catalogue

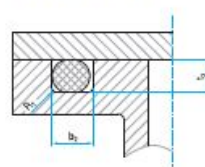
Elastomer	Označení	Tvrdost [ShA]	Teplotní rozsah
Nitrilbutadienkaučuk	NBR 60 3156 60	60	-30 °C až +70 °C
	NBR 70	70	-30 °C až +100 °C krátkodobě +120 °C
	NBR 80 1078 80	80	-40 °C až +125 °C
	NBR 80 31582 80	80	-25 °C až +80 °C krátkodobě +100 °C
	NBR 80 45802	80	-40 °C až +100 °C krátkodobě +120 °C
	NBR 90	90	-25 °C až +100 °C krátkodobě +120 °C
Fluorkaučuk	FPM 80	80	-20 °C až +220 °C
Silikonkaučuk	MVQ 50	50	-55 °C až +180 °C
	MVQ 60	60	-55 °C až +180 °C
	MVQ 70	70	-55 °C až +180 °C
	MVQ 80	80	-55 °C až +180 °C
Polyuretan	AU 90 8159	90	-25 °C až +80 °C
Etylenpropylenkaučuk	EPDM 70	70	-40 °C až + 130 °C

Obdélníková drážka

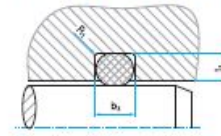
Těsnění statické - radiální



Těsnění statické - axiální



Těsnění hydraulické - pneumatické



Průměr průřezu d_2 [mm]	Statická aplikace [mm]				Dynamická aplikace [mm]				Poioměr R_1 [mm]
	radiálně		axiálně		hydraulika		pneumatika		
	$t_1 +0,05$	$b_1 +0,25$	$t_2 +0,05$	$b_2 +0,25$	$t_3 +0,05$	$b_3 +0,25$	$t_3 +0,05$	$b_3 +0,25$	
1,00	0,8	1,3	0,75	1,4	0,9	1,3	0,95	1,2	0,3
1,25	0,9	1,7	0,90	1,7	1,1	1,6	1,15	1,5	0,3
1,50	1,1	2,0	1,10	2,1	1,3	1,9	1,35	1,8	0,3
1,78	1,3	2,4	1,30	2,5	1,5	2,3	1,55	2,2	0,3
1,80	1,3	2,4	1,30	2,6	1,5	2,4	1,55	2,3	0,3
2,00	1,5	2,6	1,50	2,8	1,7	2,6	1,75	2,4	0,3
2,20	1,7	3,0	1,60	3,1	1,9	2,8	2,00	2,6	0,3
2,40	1,8	3,2	1,80	3,3	2,1	3,0	2,15	2,9	0,3
2,50	1,9	3,3	1,90	3,5	2,2	3,1	2,25	3,0	0,3
2,62	2,0	3,5	2,00	3,7	2,2	3,4	2,35	3,1	0,4
2,65	2,0	3,6	2,00	3,8	2,3	3,4	2,35	3,2	0,4
3,00	2,3	3,9	2,30	4,1	2,6	3,8	2,70	3,6	0,5
3,50	2,7	4,6	2,70	4,8	3,1	4,4	3,15	4,2	0,5
3,53	2,7	4,7	2,70	4,9	3,1	4,5	3,20	4,3	0,5
3,55	2,8	4,7	2,70	5,0	3,1	4,5	3,20	4,3	0,5
4,00	3,2	5,2	3,10	5,5	3,5	5,1	3,65	4,8	0,6
4,50	3,6	5,8	3,50	6,1	4,0	5,7	4,20	5,4	0,6
5,00	4,0	6,5	4,00	6,7	4,4	6,4	4,65	5,9	0,6
5,30	4,3	7,0	4,20	7,2	4,7	6,8	4,95	6,4	0,6
5,33	4,3	7,1	4,20	7,3	4,7	6,9	4,95	6,4	0,6
5,50	4,5	7,2	4,50	7,4	4,9	7,1	5,15	6,5	0,7
5,70	4,6	7,6	4,60	7,6	5,1	7,2	5,35	6,8	0,7
6,00	4,9	7,9	4,80	8,2	5,4	7,5	5,60	7,2	0,8
6,50	5,4	8,4	5,30	8,6	5,8	8,1	6,15	7,8	0,8
6,99	5,8	9,2	5,70	9,7	6,2	8,8	6,55	8,3	0,8
7,00	5,8	9,3	5,70	9,7	6,2	8,9	6,60	8,4	0,8
7,50	6,3	9,8	6,20	10,1	6,7	9,4	7,10	8,9	0,8
8,00	6,7	10,5	6,60	10,7	7,1	10,2	7,60	9,5	0,9
8,50	7,2	11,0	7,20	11,3	7,6	10,8	8,00	10,2	1,0
9,00	7,7	11,7	7,60	12,0	8,1	11,4	8,50	10,8	1,0
9,50	8,2	12,3	8,10	12,5	8,5	12,0	9,00	11,4	1,0
10,00	8,6	13,0	8,50	13,6	10,0	12,6	9,50	12,0	1,0